ภาคผนวก ก

JCPDF

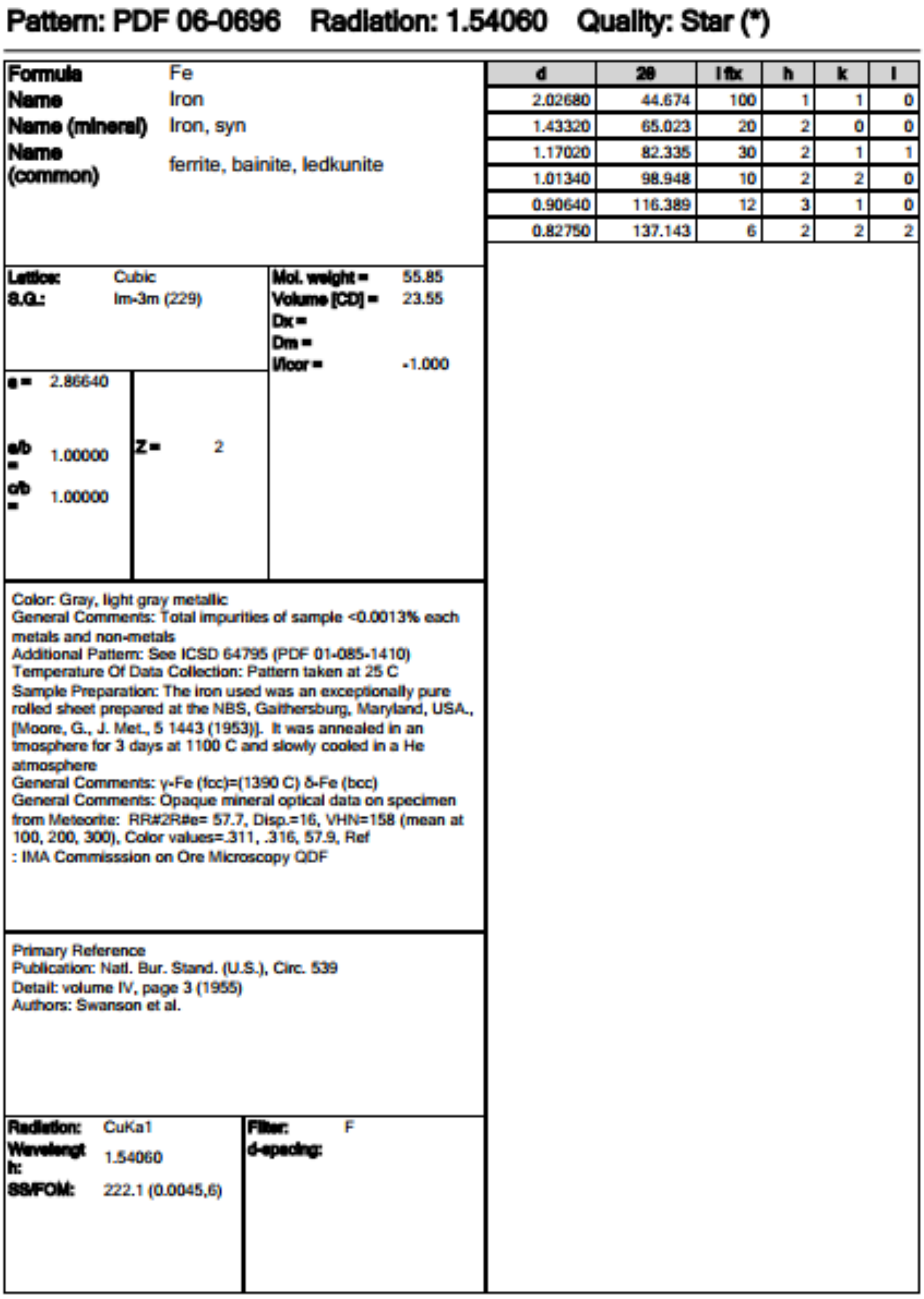

Pattern: PDF 06-0696 Radiation: 1.54060 Quality: Star (*)

Formula Fe
Name Iron
Name (mineral) Iron, syn
Name (common) ferrite, bainite, ledkunite

d	2θ	I fix	h	k	l
2.02680	44.674	100	1	1	0
1.43320	65.023	20	2	0	0
1.17020	82.335	30	2	1	1
1.01340	98.948	10	2	2	0
0.90640	116.389	12	3	1	0
0.82750	137.143	6	2	2	2

Lattice: Cubic
S.G.: Im-3m (229)

Mol. weight = 55.85
Volume [CD] = 23.55
Dx =
Dm =
I/Icor = -1.000

a = 2.86640
a/b = 1.00000
c/b = 1.00000

Z = 2

Color: Gray, light gray metallic
General Comments: Total impurities of sample <0.0013% each metals and non-metals
Additional Pattern: See ICSD 64795 (PDF 01-085-1410)
Temperature Of Data Collection: Pattern taken at 25 C
Sample Preparation: The iron used was an exceptionally pure rolled sheet prepared at the NBS, Gaithersburg, Maryland, USA., [Moore, G., J. Met., 5 1443 (1953)]. It was annealed in an tmosphere for 3 days at 1100 C and slowly cooled in a He atmosphere
General Comments: γ-Fe (fcc)=(1390 C) δ-Fe (bcc)
General Comments: Opaque mineral optical data on specimen from Meteorite: RR#2R#e= 57.7, Disp.=16, VHN=158 (mean at 100, 200, 300), Color values=.311, .316, 57.9, Ref : IMA Commisssion on Ore Microscopy QDF

Primary Reference
Publication: Natl. Bur. Stand. (U.S.), Circ. 539
Detail: volume IV, page 3 (1955)
Authors: Swanson et al.

Radiation: CuKa1
Wavelength: 1.54060
SS/FOM: 222.1 (0.0045,6)

Filter: F
d-spacing:

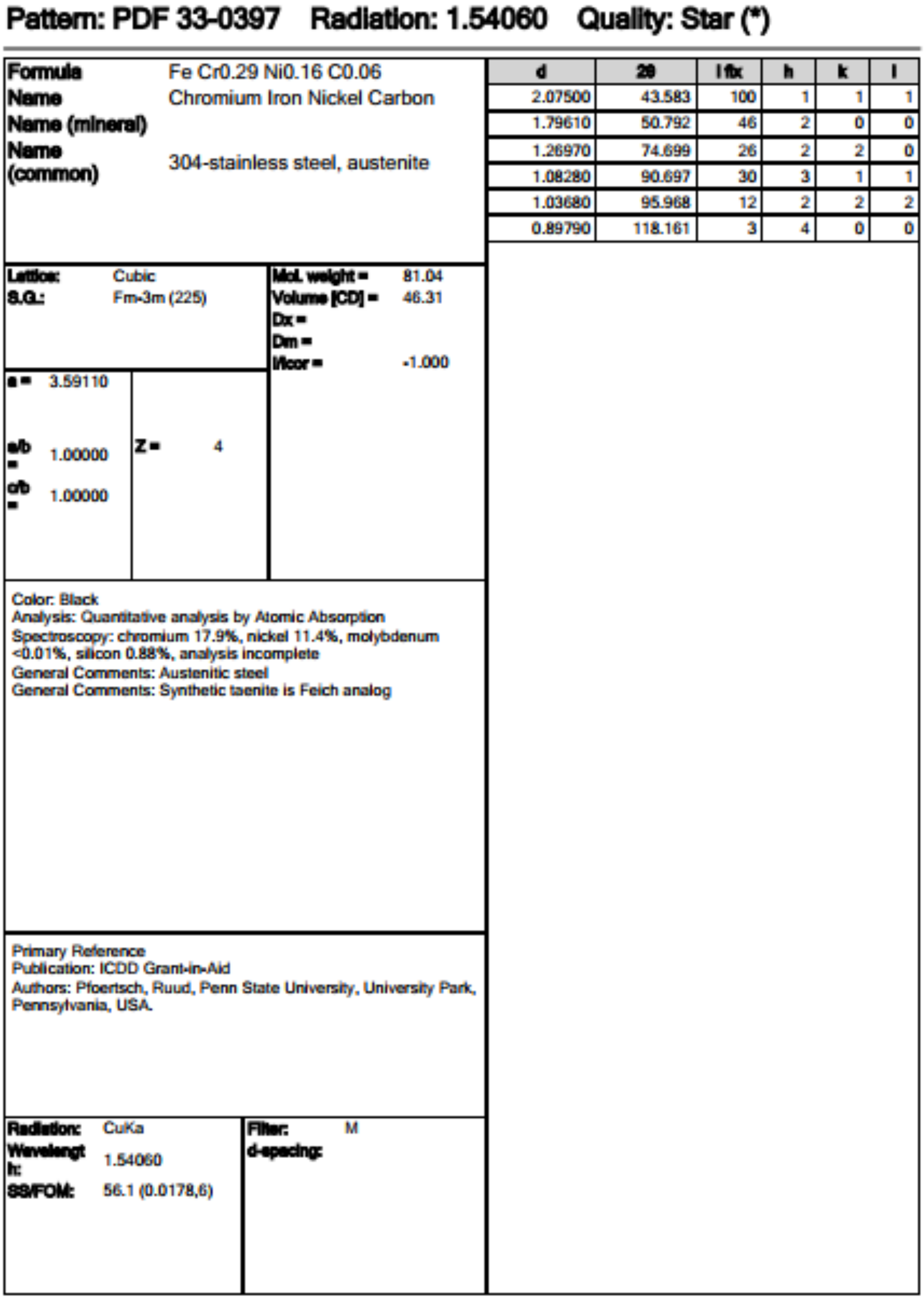

Pattern: PDF 33-0397 Radiation: 1.54060 Quality: Star (*)

Formula Fe Cr0.29 Ni0.16 C0.06
Name Chromium Iron Nickel Carbon
Name (mineral)
Name (common) 304-stainless steel, austenite

Lattice: Cubic
S.G.: Fm-3m (225)

Mol. weight = 81.04
Volume [CD] = 46.31
Dx =
Dm =
I/Icor = -1.000

a = 3.59110
a/b = 1.00000
c/b = 1.00000
Z = 4

Color: Black
Analysis: Quantitative analysis by Atomic Absorption Spectroscopy: chromium 17.9%, nickel 11.4%, molybdenum <0.01%, silicon 0.88%, analysis incomplete
General Comments: Austenitic steel
General Comments: Synthetic taenite is Feich analog

Primary Reference
Publication: ICDD Grant-in-Aid
Authors: Pfoertsch, Ruud, Penn State University, University Park, Pennsylvania, USA.

Radiation: CuKa
Wavelength: 1.54060
SS/FOM: 56.1 (0.0178,6)
Filter: M
d-spacing:

d	2θ	I fix	h	k	l
2.07500	43.583	100	1	1	1
1.79610	50.792	46	2	0	0
1.26970	74.699	26	2	2	0
1.08280	90.697	30	3	1	1
1.03680	95.968	12	2	2	2
0.89790	118.161	3	4	0	0

Pattern: PDF 39-1346 Radiation: 1.54060 Quality: Star (*)

Formula Fe2 O3
Name Iron Oxide
Name (mineral) Maghemite-C, syn
Name (common)

Lattice: Cubic
S.G.: P4132 (213)

Mol. weight = 159.69
Volume [CD] = 582.5
Dx =
Dm = 4.9
I/Icor = 1.400

a = 8.35150
a/b = 1.00000
c/b = 1.00000
Z = 11

Color: Light brown
Sample Source Or Locality: Sample from Control Data as used in hard disks
Optical Data: B=2.74
General Comments: Optical data on specimen from Iron Mountain, Shasta County, California, USA
Sample Preparation: Space group dependent upon preparation (Bernal et al.)
Additional Pattern: To replace 00-004-0755 and 00-024-0081
General Comments: Pattern reviewed by Syvinski, W., McCarthy, G., North Dakota State University, Fargo, North Dakota, USA, ICDD Grant-in-Aid (1990). Agrees well with experimental pattern. Additional weak reflections [indicated by brackets] were observed

Primary Reference
Publication: ICDD Grant-in-Aid
Authors: Schulz, D., McCarthy, G., North Dakota State University, Fargo, North Dakota, USA.

Radiation: CuKa
Wavelength: 1.54060
SS/FOM: 94.9 (0.009,35)
Filter: M
d-spacing:

d	2θ	I fix	h	k	l
5.91800	14.958	6	1	1	0
4.82200	18.384	4	1	1	1
3.74000	23.772	6	2	1	0
3.41100	26.103	6	2	1	1
2.95300	30.241	35	2	2	0
2.78400	32.125	2	2	2	1
2.64350	33.883	2	3	1	0
2.51770	35.631	100	3	1	1
2.41190	37.250	3	2	2	2
2.31630	38.848	1	3	2	0
2.23200	40.378	1	3	2	1
2.08860	43.285	16	4	0	0
2.02550	44.705	1	4	1	0
1.96850	46.072	1	3	3	0
1.82240	50.008	2	4	2	1
1.70450	53.734	11	4	2	2
1.67030	54.926	1	4	3	0
1.63790	56.107	1	5	1	0
1.60730	57.273	24	5	1	1
1.55070	59.569	1	5	2	0
1.52480	60.687	2	5	2	1
1.47580	62.927	34	4	4	0
1.45370	63.996	1	4	4	1
1.43220	65.074	1	5	3	0
1.39190	67.203	1	4	4	2
1.37300	68.255	1	6	1	0
1.35470	69.307	1	6	1	1
1.32040	71.378	3	6	2	0
1.30420	72.403	1	5	4	0
1.27300	74.473	6	5	3	3
1.25900	75.444	2	6	2	2
1.24500	76.445	1	6	3	0
1.23140	77.445	1	6	3	1
1.20530	79.448	1	4	4	4
1.19310	80.426	1	6	3	2
1.18100	81.422	1	7	1	0
1.13650	85.341	1	7	2	1
1.11590	87.307	2	6	4	2
1.09660	89.247	1	7	3	0
1.08720	90.229	7	7	3	1
1.04390	95.106	3	8	0	0

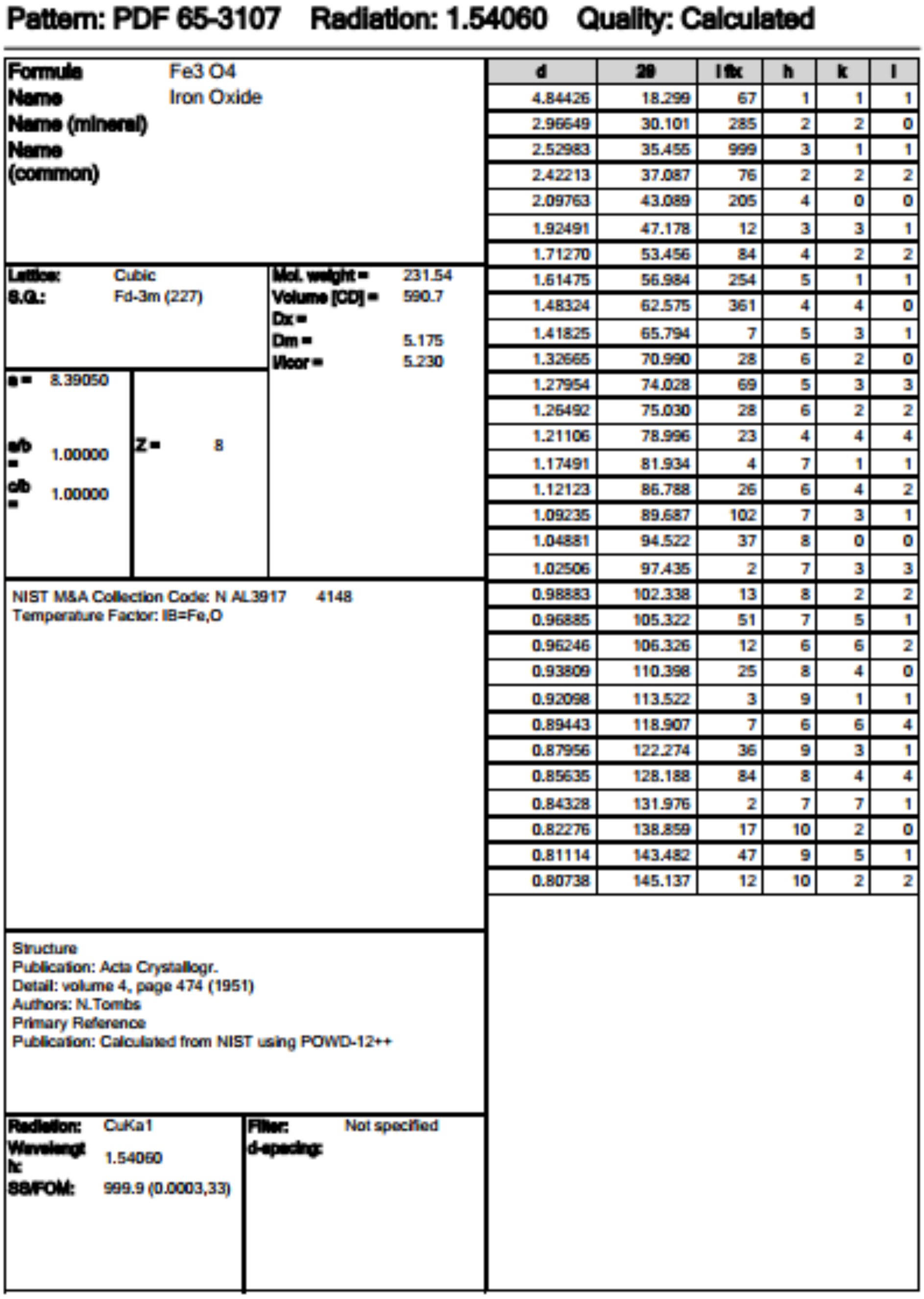

Pattern: PDF 65-3107 Radiation: 1.54060 Quality: Calculated

Formula	Fe3 O4
Name	Iron Oxide
Name (mineral)	
Name (common)	

Lattice:	Cubic	**Mol. weight =**	231.54
S.G.:	Fd-3m (227)	**Volume [CD] =**	590.7
		Dx =	
		Dm =	5.175
		Vicor =	5.230

a =	8.39050	**Z =**	8
a/b =	1.00000		
c/b =	1.00000		

NIST M&A Collection Code: N AL3917 4148
Temperature Factor: IB=Fe,O

Structure
Publication: Acta Crystallogr.
Detail: volume 4, page 474 (1951)
Authors: N.Tombs
Primary Reference
Publication: Calculated from NIST using POWD-12++

Radiation:	CuKa1	**Filter:**	Not specified
Wavelength:	1.54060	**d-spacing:**	
SS/FOM:	999.9 (0.0003,33)		

d	2θ	I fix	h	k	l
4.84426	18.299	67	1	1	1
2.96649	30.101	285	2	2	0
2.52983	35.455	999	3	1	1
2.42213	37.087	76	2	2	2
2.09763	43.089	205	4	0	0
1.92491	47.178	12	3	3	1
1.71270	53.456	84	4	2	2
1.61475	56.984	254	5	1	1
1.48324	62.575	361	4	4	0
1.41825	65.794	7	5	3	1
1.32665	70.990	28	6	2	0
1.27954	74.028	69	5	3	3
1.26492	75.030	28	6	2	2
1.21106	78.996	23	4	4	4
1.17491	81.934	4	7	1	1
1.12123	86.788	26	6	4	2
1.09235	89.687	102	7	3	1
1.04881	94.522	37	8	0	0
1.02506	97.435	2	7	3	3
0.98883	102.338	13	8	2	2
0.96885	105.322	51	7	5	1
0.96246	106.326	12	6	6	2
0.93809	110.398	25	8	4	0
0.92098	113.522	3	9	1	1
0.89443	118.907	7	6	6	4
0.87956	122.274	36	9	3	1
0.85635	128.188	84	8	4	4
0.84328	131.976	2	7	7	1
0.82276	138.859	17	10	2	0
0.81114	143.482	47	9	5	1
0.80738	145.137	12	10	2	2

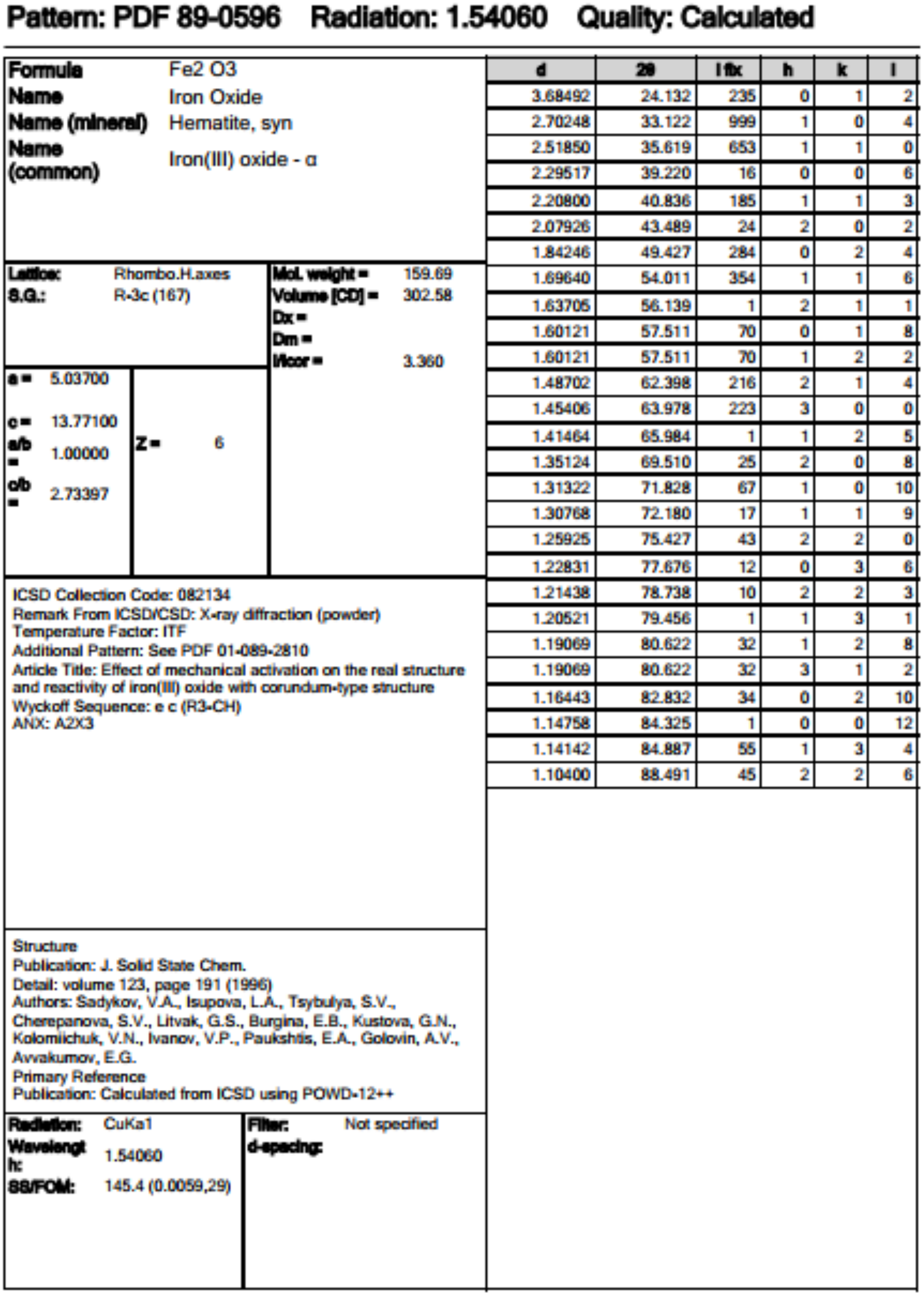

Pattern: PDF 89-0596 Radiation: 1.54060 Quality: Calculated

Formula Fe2 O3
Name Iron Oxide
Name (mineral) Hematite, syn
Name (common) Iron(III) oxide - α

Lattice: Rhombo.H.axes
S.G.: R-3c (167)

Mol. weight = 159.69
Volume [CD] = 302.58
Dx =
Dm =
I/Icor = 3.360

a = 5.03700
c = 13.77100
a/b = 1.00000
c/b = 2.73397
Z = 6

ICSD Collection Code: 082134
Remark From ICSD/CSD: X-ray diffraction (powder)
Temperature Factor: ITF
Additional Pattern: See PDF 01-089-2810
Article Title: Effect of mechanical activation on the real structure and reactivity of iron(III) oxide with corundum-type structure
Wyckoff Sequence: e c (R3-CH)
ANX: A2X3

Structure
Publication: J. Solid State Chem.
Detail: volume 123, page 191 (1996)
Authors: Sadykov, V.A., Isupova, L.A., Tsybulya, S.V., Cherepanova, S.V., Litvak, G.S., Burgina, E.B., Kustova, G.N., Kolomiichuk, V.N., Ivanov, V.P., Paukshtis, E.A., Golovin, A.V., Avvakumov, E.G.
Primary Reference
Publication: Calculated from ICSD using POWD-12++

Radiation: CuKa1
Wavelength: 1.54060
SS/FOM: 145.4 (0.0059,29)
Filter: Not specified
d-spacing:

d	2θ	I fix	h	k	l
3.68492	24.132	235	0	1	2
2.70248	33.122	999	1	0	4
2.51850	35.619	653	1	1	0
2.29517	39.220	16	0	0	6
2.20800	40.836	185	1	1	3
2.07926	43.489	24	2	0	2
1.84246	49.427	284	0	2	4
1.69640	54.011	354	1	1	6
1.63705	56.139	1	2	1	1
1.60121	57.511	70	0	1	8
1.60121	57.511	70	1	2	2
1.48702	62.398	216	2	1	4
1.45406	63.978	223	3	0	0
1.41464	65.984	1	1	2	5
1.35124	69.510	25	2	0	8
1.31322	71.828	67	1	0	10
1.30768	72.180	17	1	1	9
1.25925	75.427	43	2	2	0
1.22831	77.676	12	0	3	6
1.21438	78.738	10	2	2	3
1.20521	79.456	1	1	3	1
1.19069	80.622	32	1	2	8
1.19069	80.622	32	3	1	2
1.16443	82.832	34	0	2	10
1.14758	84.325	1	0	0	12
1.14142	84.887	55	1	3	4
1.10400	88.491	45	2	2	6

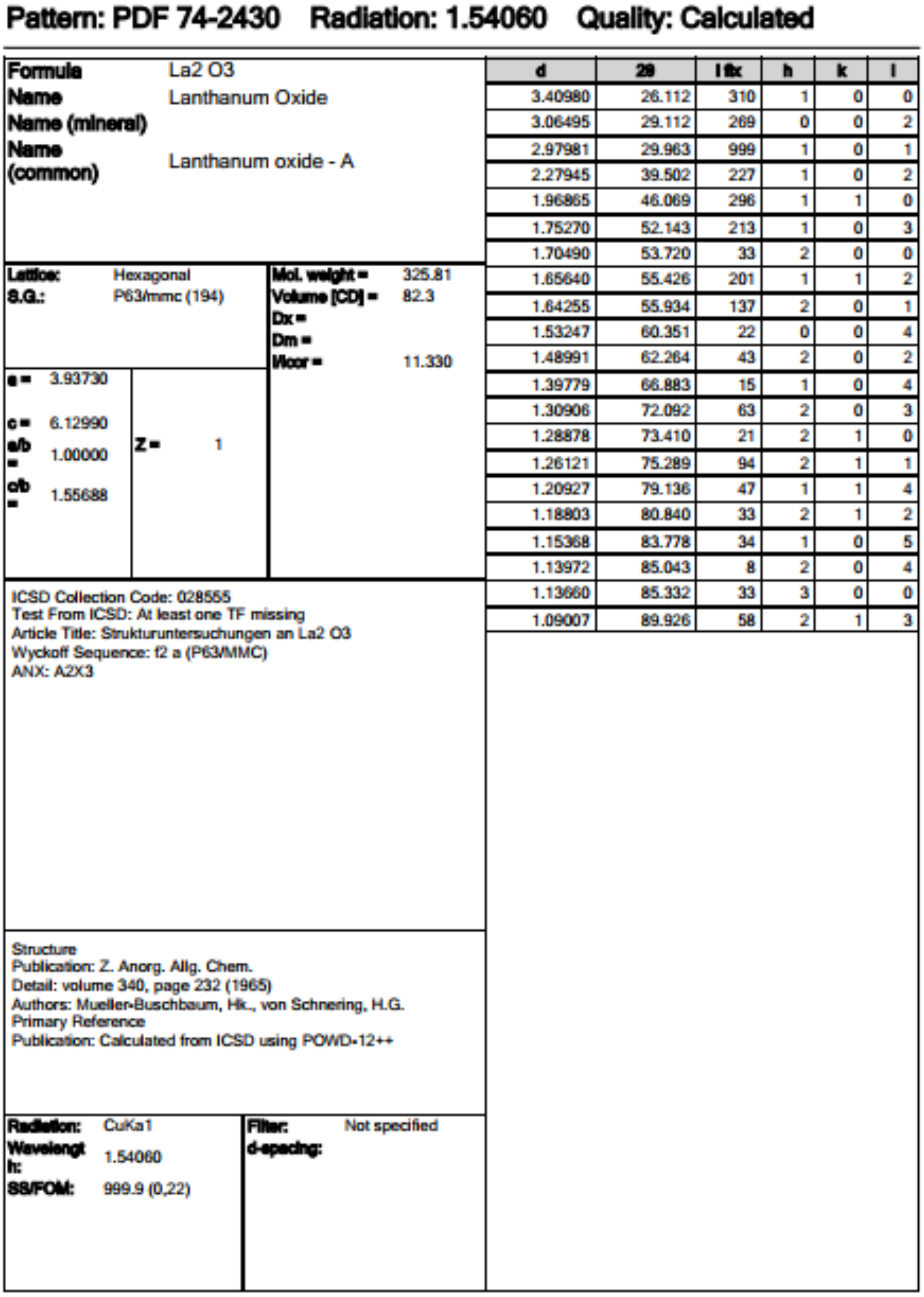

Pattern: PDF 74-2430 Radiation: 1.54060 Quality: Calculated

Formula La2 O3
Name Lanthanum Oxide
Name (mineral)
Name (common) Lanthanum oxide - A

Lattice: Hexagonal
S.G.: P63/mmc (194)

Mol. weight = 325.81
Volume [CD] = 82.3
Dx =
Dm =
I/Icor = 11.330

a = 3.93730
c = 6.12990
a/b = 1.00000
c/b = 1.55688

Z = 1

ICSD Collection Code: 028555
Test From ICSD: At least one TF missing
Article Title: Strukturuntersuchungen an La2 O3
Wyckoff Sequence: f2 a (P63/MMC)
ANX: A2X3

Structure
Publication: Z. Anorg. Allg. Chem.
Detail: volume 340, page 232 (1965)
Authors: Mueller-Buschbaum, Hk., von Schnering, H.G.
Primary Reference
Publication: Calculated from ICSD using POWD-12++

Radiation: CuKa1
Wavelength: 1.54060
SS/FOM: 999.9 (0,22)

Filter: Not specified
d-spacing:

d	2θ	I fix	h	k	l
3.40980	26.112	310	1	0	0
3.06495	29.112	269	0	0	2
2.97981	29.963	999	1	0	1
2.27945	39.502	227	1	0	2
1.96865	46.069	296	1	1	0
1.75270	52.143	213	1	0	3
1.70490	53.720	33	2	0	0
1.65640	55.426	201	1	1	2
1.64255	55.934	137	2	0	1
1.53247	60.351	22	0	0	4
1.48991	62.264	43	2	0	2
1.39779	66.883	15	1	0	4
1.30906	72.092	63	2	0	3
1.28878	73.410	21	2	1	0
1.26121	75.289	94	2	1	1
1.20927	79.136	47	1	1	4
1.18803	80.840	33	2	1	2
1.15368	83.778	34	1	0	5
1.13972	85.043	8	2	0	4
1.13660	85.332	33	3	0	0
1.09007	89.926	58	2	1	3

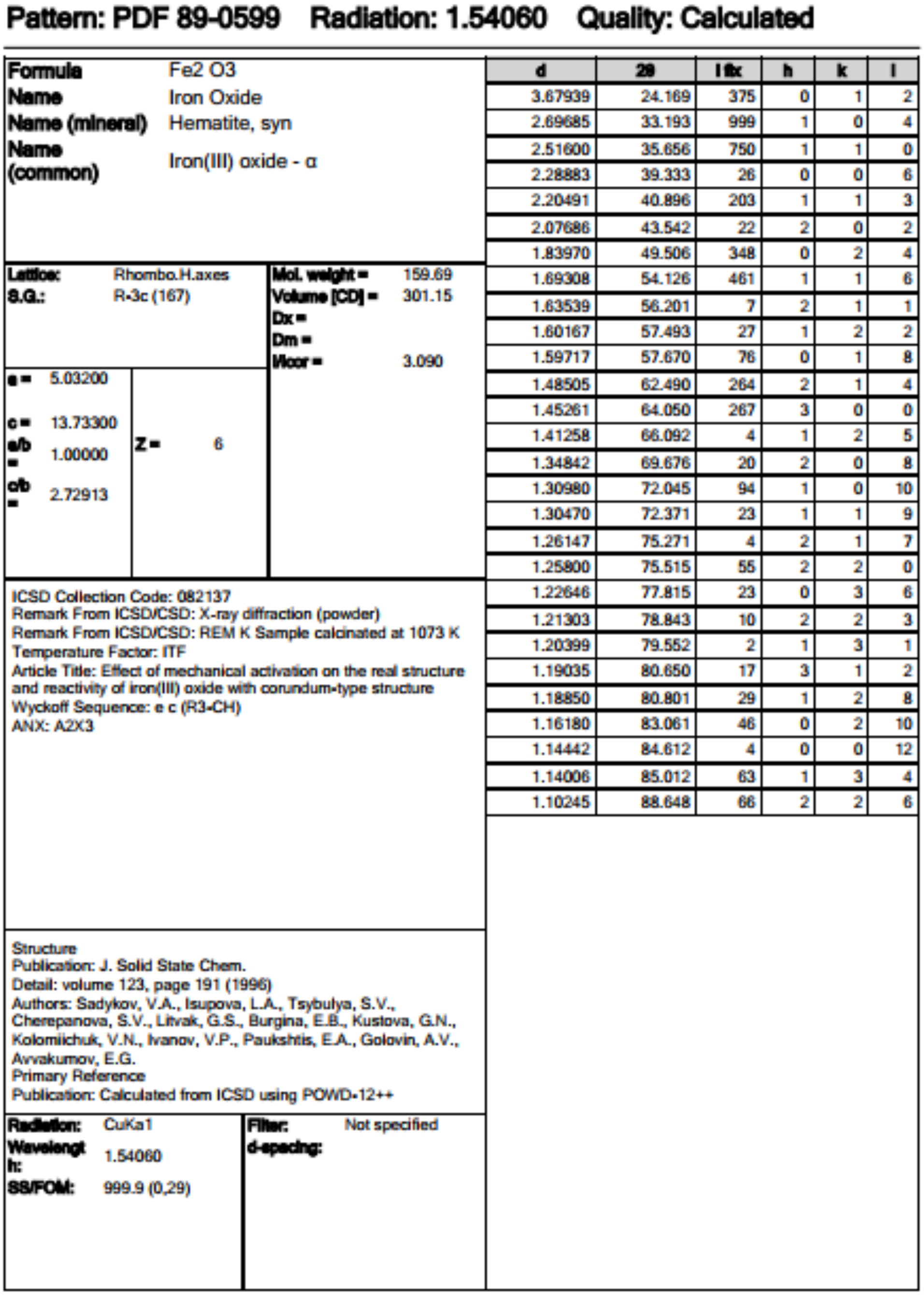

Pattern: PDF 89-0599 Radiation: 1.54060 Quality: Calculated

Formula Fe2 O3
Name Iron Oxide
Name (mineral) Hematite, syn
Name (common) Iron(III) oxide - α

Lattice: Rhombo.H.axes
S.G.: R-3c (167)

Mol. weight = 159.69
Volume [CD] = 301.15
Dx =
Dm =
I/Icor = 3.090

a = 5.03200
c = 13.73300
a/b = 1.00000
c/b = 2.72913
Z = 6

ICSD Collection Code: 082137
Remark From ICSD/CSD: X-ray diffraction (powder)
Remark From ICSD/CSD: REM K Sample calcinated at 1073 K
Temperature Factor: ITF
Article Title: Effect of mechanical activation on the real structure and reactivity of iron(III) oxide with corundum-type structure
Wyckoff Sequence: e c (R3-CH)
ANX: A2X3

Structure
Publication: J. Solid State Chem.
Detail: volume 123, page 191 (1996)
Authors: Sadykov, V.A., Isupova, L.A., Tsybulya, S.V., Cherepanova, S.V., Litvak, G.S., Burgina, E.B., Kustova, G.N., Kolomiichuk, V.N., Ivanov, V.P., Paukshtis, E.A., Golovin, A.V., Avvakumov, E.G.
Primary Reference
Publication: Calculated from ICSD using POWD-12++

Radiation: CuKa1
Wavelength: 1.54060
SS/FOM: 999.9 (0,29)
Filter: Not specified
d-spacing:

d	2θ	I fix	h	k	l
3.67939	24.169	375	0	1	2
2.69685	33.193	999	1	0	4
2.51600	35.656	750	1	1	0
2.28883	39.333	26	0	0	6
2.20491	40.896	203	1	1	3
2.07686	43.542	22	2	0	2
1.83970	49.506	348	0	2	4
1.69308	54.126	461	1	1	6
1.63539	56.201	7	2	1	1
1.60167	57.493	27	1	2	2
1.59717	57.670	76	0	1	8
1.48505	62.490	264	2	1	4
1.45261	64.050	267	3	0	0
1.41258	66.092	4	1	2	5
1.34842	69.676	20	2	0	8
1.30980	72.045	94	1	0	10
1.30470	72.371	23	1	1	9
1.26147	75.271	4	2	1	7
1.25800	75.515	55	2	2	0
1.22646	77.815	23	0	3	6
1.21303	78.843	10	2	2	3
1.20399	79.552	2	1	3	1
1.19035	80.650	17	3	1	2
1.18850	80.801	29	1	2	8
1.16180	83.061	46	0	2	10
1.14442	84.612	4	0	0	12
1.14006	85.012	63	1	3	4
1.10245	88.648	66	2	2	6

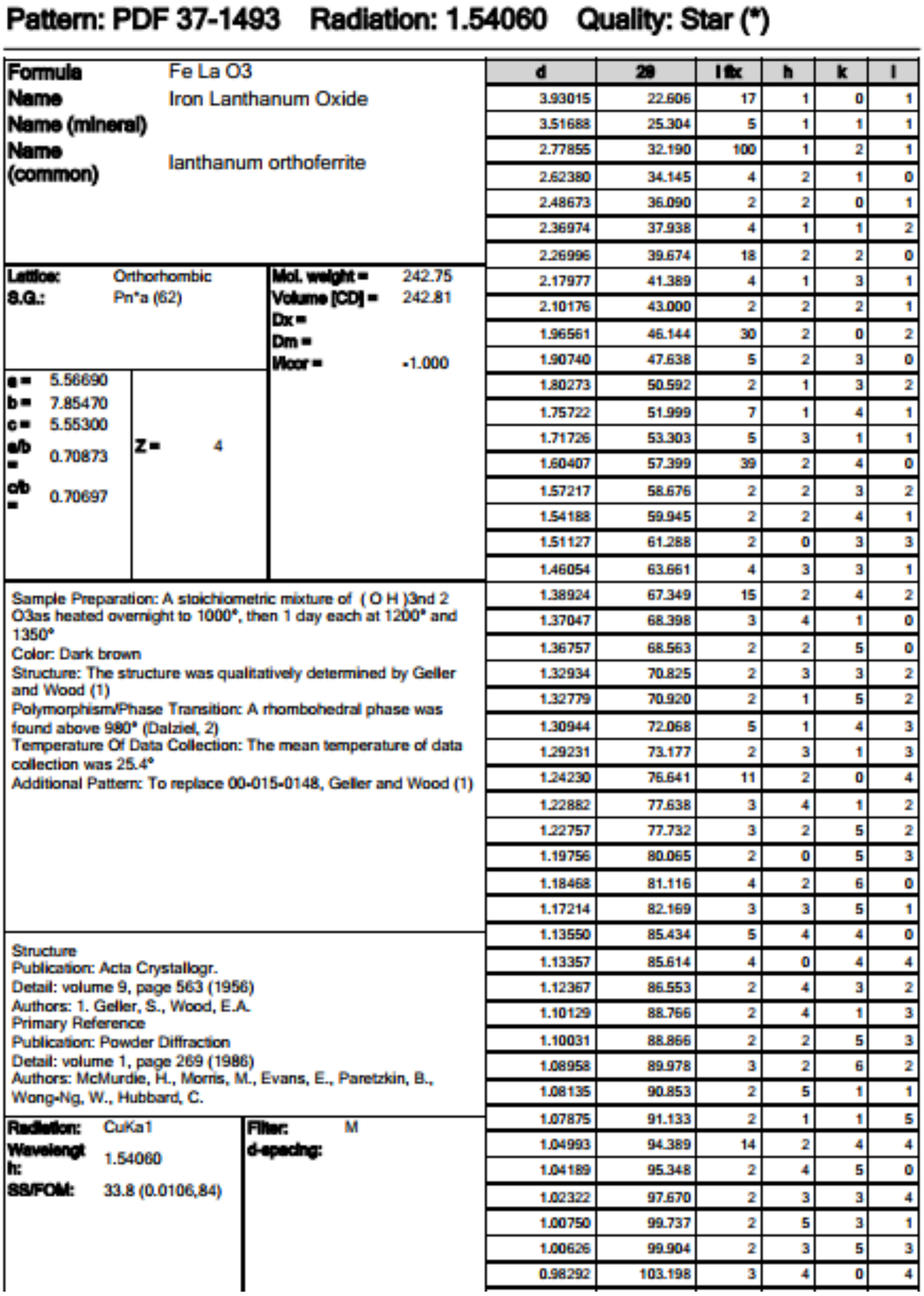

Pattern: PDF 37-1493   Radiation: 1.54060   Quality: Star (*)

Formula Fe La O3
Name Iron Lanthanum Oxide
Name (mineral)
Name (common) lanthanum orthoferrite

Lattice: Orthorhombic
S.G.: Pn*a (62)

Mol. weight = 242.75
Volume [CD] = 242.81
Dx =
Dm =
I/Icor = -1.000

a = 5.56690
b = 7.85470
c = 5.55300
a/b = 0.70873
c/b = 0.70697

Z = 4

Sample Preparation: A stoichiometric mixture of (O H)3nd 2 O3as heated overnight to 1000°, then 1 day each at 1200° and 1350°
Color: Dark brown
Structure: The structure was qualitatively determined by Geller and Wood (1)
Polymorphism/Phase Transition: A rhombohedral phase was found above 980° (Dalziel, 2)
Temperature Of Data Collection: The mean temperature of data collection was 25.4°
Additional Pattern: To replace 00-015-0148, Geller and Wood (1)

Structure
Publication: Acta Crystallogr.
Detail: volume 9, page 563 (1956)
Authors: 1. Geller, S., Wood, E.A.
Primary Reference
Publication: Powder Diffraction
Detail: volume 1, page 269 (1986)
Authors: McMurdie, H., Morris, M., Evans, E., Paretzkin, B., Wong-Ng, W., Hubbard, C.

Radiation: CuKa1
Wavelength: 1.54060
SS/FOM: 33.8 (0.0106,84)

Filter: M
d-spacing:

d	2θ	I fix	h	k	l
3.93015	22.606	17	1	0	1
3.51688	25.304	5	1	1	1
2.77855	32.190	100	1	2	1
2.62380	34.145	4	2	1	0
2.48673	36.090	2	2	0	1
2.36974	37.938	4	1	1	2
2.26996	39.674	18	2	2	0
2.17977	41.389	4	1	3	1
2.10176	43.000	2	2	2	1
1.96561	46.144	30	2	0	2
1.90740	47.638	5	2	3	0
1.80273	50.592	2	1	3	2
1.75722	51.999	7	1	4	1
1.71726	53.303	5	3	1	1
1.60407	57.399	39	2	4	0
1.57217	58.676	2	2	3	2
1.54188	59.945	2	2	4	1
1.51127	61.288	2	0	3	3
1.46054	63.661	4	3	3	1
1.38924	67.349	15	2	4	2
1.37047	68.398	3	4	1	0
1.36757	68.563	2	2	5	0
1.32934	70.825	2	3	3	2
1.32779	70.920	2	1	5	2
1.30944	72.068	5	1	4	3
1.29231	73.177	2	3	1	3
1.24230	76.641	11	2	0	4
1.22882	77.638	3	4	1	2
1.22757	77.732	3	2	5	2
1.19756	80.065	2	0	5	3
1.18468	81.116	4	2	6	0
1.17214	82.169	3	3	5	1
1.13550	85.434	5	4	4	0
1.13357	85.614	4	0	4	4
1.12367	86.553	2	4	3	2
1.10129	88.766	2	4	1	3
1.10031	88.866	2	2	5	3
1.08958	89.978	3	2	6	2
1.08135	90.853	2	5	1	1
1.07875	91.133	2	1	1	5
1.04993	94.389	14	2	4	4
1.04189	95.348	2	4	5	0
1.02322	97.670	2	3	3	4
1.00750	99.737	2	5	3	1
1.00626	99.904	2	3	5	3
0.98292	103.198	3	4	0	4

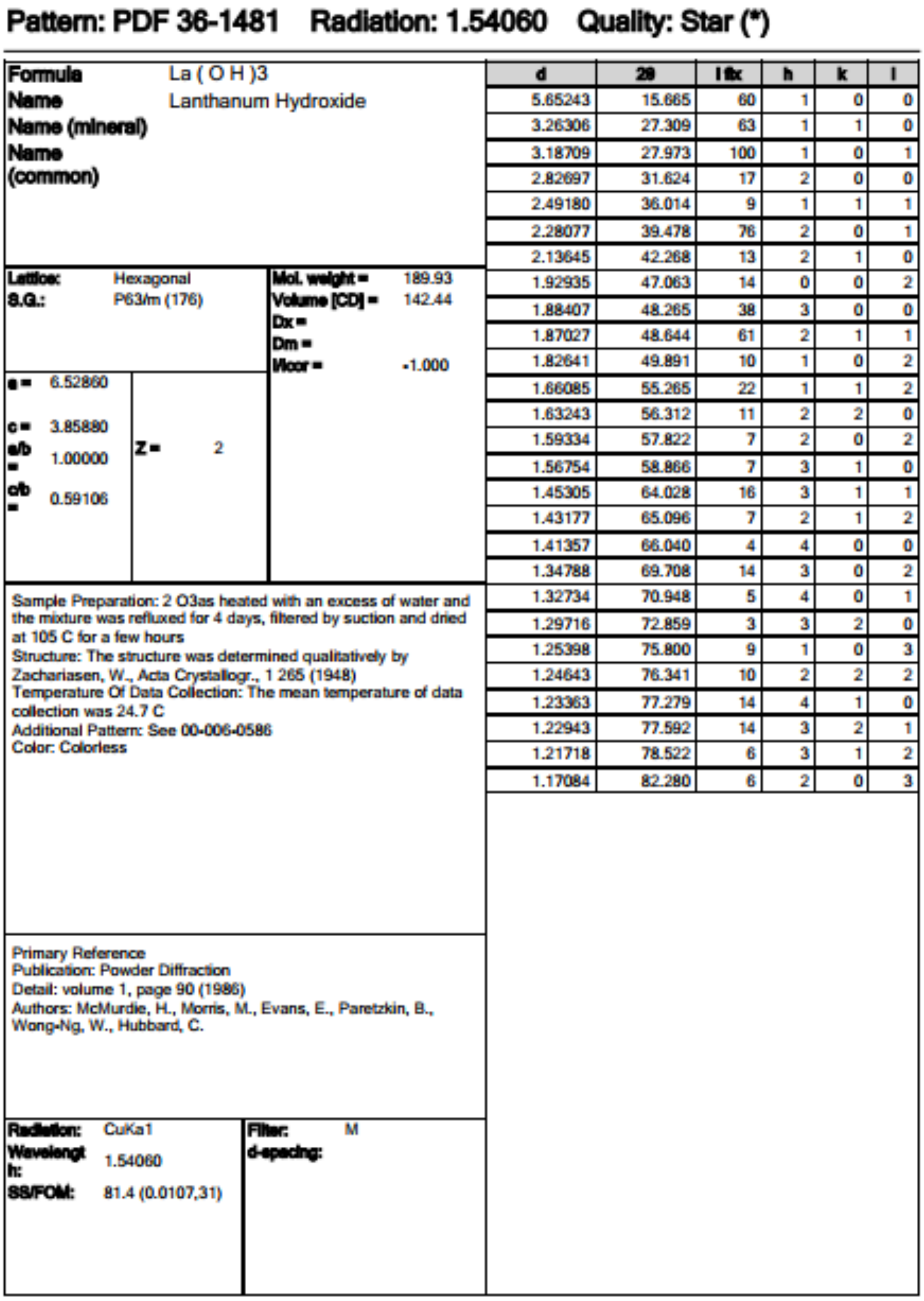

Pattern: PDF 36-1481 Radiation: 1.54060 Quality: Star (*)

Formula $La(OH)_3$
Name Lanthanum Hydroxide
Name (mineral)
Name (common)

Lattice: Hexagonal
S.G.: P63/m (176)

Mol. weight = 189.93
Volume [CD] = 142.44
Dx =
Dm =
I/Icor = -1.000

a = 6.52860
c = 3.85880
a/b = 1.00000
c/b = 0.59106
Z = 2

Sample Preparation: 2 O3as heated with an excess of water and the mixture was refluxed for 4 days, filtered by suction and dried at 105 C for a few hours
Structure: The structure was determined qualitatively by Zachariasen, W., Acta Crystallogr., 1 265 (1948)
Temperature Of Data Collection: The mean temperature of data collection was 24.7 C
Additional Pattern: See 00-006-0586
Color: Colorless

Primary Reference
Publication: Powder Diffraction
Detail: volume 1, page 90 (1986)
Authors: McMurdie, H., Morris, M., Evans, E., Paretzkin, B., Wong-Ng, W., Hubbard, C.

Radiation: CuKa1
Wavelength: 1.54060
SS/FOM: 81.4 (0.0107,31)

Filter: M
d-spacing:

d	2θ	I fix	h	k	l
5.65243	15.665	60	1	0	0
3.26306	27.309	63	1	1	0
3.18709	27.973	100	1	0	1
2.82697	31.624	17	2	0	0
2.49180	36.014	9	1	1	1
2.28077	39.478	76	2	0	1
2.13645	42.268	13	2	1	0
1.92935	47.063	14	0	0	2
1.88407	48.265	38	3	0	0
1.87027	48.644	61	2	1	1
1.82641	49.891	10	1	0	2
1.66085	55.265	22	1	1	2
1.63243	56.312	11	2	2	0
1.59334	57.822	7	2	0	2
1.56754	58.866	7	3	1	0
1.45305	64.028	16	3	1	1
1.43177	65.096	7	2	1	2
1.41357	66.040	4	4	0	0
1.34788	69.708	14	3	0	2
1.32734	70.948	5	4	0	1
1.29716	72.859	3	3	2	0
1.25398	75.800	9	1	0	3
1.24643	76.341	10	2	2	2
1.23363	77.279	14	4	1	0
1.22943	77.592	14	3	2	1
1.21718	78.522	6	3	1	2
1.17084	82.280	6	2	0	3

ภาคผนวก ข

บทความทางวิชาการที่ได้รับการเผยแพร่ในระหว่างการศึกษา

Ceramics International 50 (2024) 44268–44278

Contents lists available at ScienceDirect

Ceramics International

journal homepage: www.elsevier.com/locate/ceramint

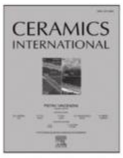

Utilizing acid-etched Fe-waste for sustainable synthesis of conductive perovskite-type materials from automotive industrial residue

Siriwan Chokkha [*], Aphisit Tonsanthia, Natthawat Chuprasoet, Kraiwut Rukkachat

School of Ceramic Engineering, Institute of Engineering, Suranaree University of Technology, Nakhon Ratchasima, 30000, Thailand

ARTICLE INFO

Handling editor: P. Vincenzini

ABSTRACT

A common method for reducing waste and environmental problems brought on by landfills is to reuse waste, especially heavy metals such as iron. Automotive industrial waste containing Fe-rich metal is successfully transformed into a highly pure structure of Fe_2O_3 using an etching method with HNO_3 acid. This resulting structure serves as a precursor for synthesizing $LaNi_{1-x}Fe_xO_{3\pm\delta}$ perovskite conducting materials. The desired perovskite conductive phase can be produced by substituting Fe_2O_3-treated waste at the B-site (Ni position) before calcination at 1200 °C. However, $LaNiO_{3\pm\delta}$ and $LaNi_{0.6}Fe_{0.4}O_{3\pm\delta}$ could not be synthesized under ideal conditions, as indicated by XRD analysis using TOPAS software, which revealed the presence of undesirable phases. Both compounds, $LaNiO_{3\pm\delta}$ and $LaNi_{0.6}Fe_{0.4}O_{3\pm\delta}$ demonstrated electrical conductivity with values of 362 S/cm and 42 S/cm at 550 °C, respectively. Nonetheless, electrical conductivity of both compounds decreased due to unintended phase contamination during the synthesis process. The Fe_2O_3-substituted compounds at the Ni position, in an exact amount of 1 mol, exhibited minimal electrical conductivity. Although the synthesis conditions to produce a single phase of $LaFeO_{3\pm\delta}$ were identified, $LaFeO_{3\pm\delta}$, despite its low electrical conductivity, is frequently used in electrical devices as a gas detection sensor. The thermal expansion coefficient of all synthesized waste samples is represented in the range of 12–13 × 10^{-6} °C^{-1}, which is comparable to IT-SOFC electrolyte materials. Furthermore, microstructural investigation revealed that the introduction of Fe into $LaNiO_{3\pm\delta}$ reduced particle size and porosity, ultimately resulting in higher densities. These findings were confirmed through synchrotron radiation x-ray tomographic microscopy (SR-XTM) analysis. The research suggests that converting Fe-waste into a pure phase of Fe_2O_3 using a strong acid etching technique can serve as a viable precursor for synthesizing conductive materials. This approach enhances the value of industrial waste while also reducing its volume.

1. Introduction

The use of vehicles is crucial to human transportation activity, and as the COVID-19 crisis subsides, there are witnessing an upsurge in travel and transportation. The demand for automobiles is expected to rise [1], leading to an increase in automotive industrial waste as well. The amount of iron waste powder produced from the grinding of automobile parts is substantial. Landfilling is one method for disposing of this waste, leading to harm to the ecosystem and an increase in disposal expenses. The preliminary study and management of automotive industrial waste are based on the paper report by N. Chuprasoet et al., 2021. Contaminated waste is initially cleaned with water and then extracted using a magnet. Nitric acid (HNO_3) and hydrochloric acid (HCl) are employed to convert the chemical structure into a single phase of iron compound. However, XRD measurements revealed chemical changes caused by using HNO_3 acid, leading to the formation of intact iron oxide compounds. A new single phase of Fe_2O_3 is produced when using a chemical etching technique by soaking of Fe-iron waste in HNO_3 acid [2]. Hence, the transformation of Fe-rich iron waste into high-purity iron compounds renders it suitable for various applications, such as a starting raw material for ceramic pigments, magnetic materials, gas sensors, fuel cells cathode materials, and so on [3–6].

Fuel cells (FCs) are electrochemical devices converting fuel into electricity that are considered promising alternative energy sources with applications in stationary power plants, portable devices, vehicles, and more. Boasting high efficiency and minimal pollution, these systems produce only water and heat. Types of FCs include low-temperature fuel cells such as alkaline fuel cells, phosphoric acid fuel cells, polymer

---

* Corresponding author.
E-mail address: siriwan@sut.ac.th (S. Chokkha).

https://doi.org/10.1016/j.ceramint.2024.08.276
Received 2 January 2024; Received in revised form 14 August 2024; Accepted 17 August 2024
Available online 18 August 2024
0272-8842/© 2024 Elsevier Ltd and Techna Group S.r.l. All rights are reserved, including those for text and data mining, AI training, and similar technologies.

electrolyte membrane fuel cells and high-temperature fuel cells such as molten carbonate fuel cells at 600–700 °C and solid oxide fuel cells (SOFC) at 600–1000 °C [7–9]. Advances in materials science enhance intermediate-temperature solid oxide fuel cells (IT-SOFC) at 600–800 °C, aiming to broaden the operational temperature range, extend service life, and reduce unit cell costs. IT-SOFC exhibits high electricity production [10,11]. According to recent studies, a variety of structures are employed as cathode materials in IT-SOFC systems, with the perovskite structure being one of the most effective and long-lasting configurations. The $LaNiO_{3\pm\delta}$ perovskite material is outstanding. A.A. Yaremchenko et al. (2019) studied $LaNiO_{3\pm\delta}$ prepared via the glycine-nitrate combustion process. The electrical conductivity at 800 °C was found to be high at 450 S/cm, but it exhibited a high coefficient of thermal expansion, measuring 13.7×10^{-6} °C^{-1} at 25–900 °C [12]. Because the material's expansion characteristics do not match those of the other components in the IT-SOFC cell, using it within its working temperature range can lead to cell rupture and destruction. Therefore, the recommended solution is to substitute Fe in the Ni (B-site) position in order to reduce the expansion coefficient of $LaNiO_{3\pm\delta}$. This strategic decision is based on previous research showing that $LaFeO_{3\pm\delta}$ has a smaller expansion coefficient [13]. $LaNi1_{-x}Fe_xO_{3\pm\delta}$ was prepared by a solid-state reaction with previously studied by Reiichi Chiba et al. (1999). They found that the material had its highest electrical conductivity when x = 0.4, with a maximum electrical conductivity of 580 S/cm at 800 °C and a relatively low average coefficient of thermal expansion (11.1×10^{-6} °C^{-1}) from 30 to 800 °C [14]. The $LaNi_{0.6}Fe_{0.4}O_{3\pm\delta}$ perovskite structure was studied by R.N. Basu et al. (2004) with two combustion synthesis techniques using urea and citrate-gel. The results of the study indicated that the $LaNi_{0.6}Fe_{0.4}O_{3\pm\delta}$ samples sintered at 1200 °C for 3 h exhibited physical characteristics that included an average particle size of 0.3 μm, a density of 4.2 g/cm^3, and a porosity of 40 % when synthesized by citrate-gel. This material exhibited the highest electrical conductivity of 172.7 S/cm at 700 °C. $LaNi_{0.6}Fe_{0.4}O_{3\pm\delta}$ samples sintered at 1200 °C for 3 h revealed an average particle size of 0.7 μm, a density of 4.3 g/cm^3, and a porosity of 38 % when synthesized by the urea method. The highest electrical conductivity of $LaNi_{0.6}Fe_{0.4}O_{3\pm\delta}$ samples synthesized by the urea method is 140.8 S/cm at 700 °C. However, the coefficient of thermal expansion of both combustion synthesis from processes was found to be approximately 11.4×10^{-6} °C^{-1} at 800 °C [15]. Moreover, K. Vidal et al. (2015) studied on the $LaNi_{0.6}Fe_{0.4}O_{3\pm\delta}$ perovskite structure prepared by the glycine–nitrate route using different amounts of glycine/fuel ratio (G/N = 0.5, 1.0 and 1.5). The results indicate that a sample obtained with a G/N ratio of 1.0 exhibits more suitable conductivity values for application as an IT-SOFC contact material. The samples sintered at 1050 °C display particles with grain sizes of about 0.3–0.4 μm. It exhibited a maximum electrical conductivity of 387 S/cm at 600 °C and average coefficient of thermal expansion from 600 to 1000 °C at 12.43×10^{-6} °C^{-1}. Smaller particle sizes are advantageous for sintering and result in higher density [16]. It is evident that the $LaNi_{0.6}Fe_{0.4}O_{3\pm\delta}$ structure is well-suited as a conductive material for use as a cathode material in IT-SOFC [17,18]. This suitability stems from its high electrical conductivity at operating temperatures and a low expansion coefficient, similar to that of other fuel cell components. This positively impacts the service life and overall efficiency of IT-SOFC. However, no research has been found that incorporates recycled waste into its production process. Consequently, if waste is recycled and utilized as a starting material for synthesizing electrically conductive materials, it can contribute to a sustainable reduction of environmental problems. Moreover, this approach adds value to industrial waste.

This article focuses on the synthesis of Fe_2O_3 derived from iron (Fe), which is a waste product in the automotive parts industry from which it can be found in large quantities. This type of waste is often disposed in landfills, where it can undergo chemical changes, dissolving into ions or other forms that may contaminate water sources. If these contaminated water sources are used for human consumption, they may have negative effects on human health. The researchers became interested in the idea that if iron could be treated to achieve higher purity suitable for advanced applications and synthesized into the form of Fe_2O_3, it could be used for a wider variety of purposes. The decision to use this waste as a Solid Oxide Fuel Cell (SOFC) cathode stems from the recognition of SOFC as a high-energy and clean energy source that holds promise for future applications. From this interest, research was undertaken to confirm that the waste synthesized as Fe_2O_3 can be used to synthesize advanced materials as perovskite conductive materials, specifically the $LaNi_{1-x}Fe_xO_{3\pm\delta}$ (with x = 0, 0.4 and 1) cathode structure. This creates sustainability in terms of quality resource management and health sustainability caused by pollution. It also promotes the use of clean alternative energy such as SOFC. The approach involves doping Fe into the Ni (B-site) position to reduce the expansion coefficient properties of $LaNiO_{3\pm\delta}$. The investigation commences by analyzing the composition of industrial waste using an XRF analysis machine. Subsequently, the industrial waste undergoes a phase change study achieved by altering its chemical formula through chemical etching with HNO_3, and synthetic materials are examined via an XRD analysis machine. The initial assessment of electrical conducting properties is performed using a surface 4-probe DC at room temperature. Following this, the electrical conductivity at operational temperatures is measured using the 4-probe DC method. The expansion coefficient of the synthesized material is determined using a Dilatometer within the IT-SOFC operating temperature range, from room temperature to 800 °C. The microstructure of porous and grain distributions is then examined through FE-SEM by synchrotron light source and synchrotron radiation x-ray tomographic microscopy (SR-XTM).

2. Materials and methods

2.1. Fe-waste preparation and transformation to Fe_2O_3 by HNO_3 acid etching method

The waste powder from the grinding process in Thailand's automotive industrial sector was initially separated to remove larger contaminants such as screws, ceramic grinding plates and solid grinding stones. This separation was achieved using a sieve shaker set to a controllable size of up to 45 μm (325 mesh). In the second stage of waste treatment, oil stains resulting from contamination during the polishing process by the grinding machine were removed using water. As the last stage of waste treatment, magnetic separation was employed to remove tiny impurities from ferrous-rich waste such as non-ferrous dust and ceramic wear powder from grinding wheels. The treated iron waste was subsequently dried in an oven at 100 °C for 24 h before being manually ground to a controlled size. It was then screened through a sieve to achieve a particle size below 45 μm. The cleaned Fe-waste powder must undergo evaluation using X-ray fluorescence spectroscopy (XRF) and X-ray diffraction spectroscopy (XRD) techniques. This evaluation aims to determine the number of elements and the types of compounds present before the powder can be utilized as a precursor in the subsequent acid etching process.

Nitric acid (70 % concentrated HNO_3, Ajax Finechem) was employed as a chemical etching agent for the treated iron waste powder. Prior to the etching process, each substance was weighed according to its calculated molecular weight. The chemical reaction between the Fe-waste powder and HNO_3 took place within a laboratory chemical fume hood. The mixture was allowed to soak for 20 min to ensure the completion of the chemical reaction. The iron waste that underwent acid corrosion was subjected to a priority drying process at 100 °C. This process aimed to remove any excess water. Prior to its use as a precursor in the subsequent procedure, the transformed waste product was ground and refined using a sieve to achieve a particle size smaller than 45 μm. The successful completion of the chemical reaction during the acid etching process was confirmed through the utilization of X-ray diffraction spectroscopy (XRD) techniques.

2.2. Synthesis of $LaNi_{1-x}Fe_xO_{3\pm\delta}$ perovskite-type conductive materials from automotive industrial waste

Stoichiometric ratios of Lanthanum (III) oxide 98.0 % (La_2O_3, Ajax Finechem), Nickel (II) oxide 99.0 % (NiO, BDH), and waste powders of transformed Fe_2O_3 obtained through an acid etching process (>99.9 % analyzed by XRD using TOPAS software) were employed as the initial materials for the synthesis technique of $LaNi_{1-x}Fe_xO_{3\pm\delta}$ perovskite-type conductive materials (with x = 0, 0.4 and 1) via the conventional solid-state reaction. The hygroscopic La_2O_3 powder was handled with care. It was dried at 1000 °C for 5 h before being weighed and mixed in the grinding container. The mixture was ball milled in a polyethylene bottle containing zirconia balls for 8 h using ethanol (95.0 % C_2H_5OH, Liquor) as a dispersal vehicle. After being dried at 100 °C for 24 h, the ball-milled mixture was manually ground using a mortar and pestle. The synthesized compound was subsequently calcined in the temperature range of 800–1200 °C, as determined by Simultaneous Thermal Analysis (STA) with a focus on monitoring weight changes and identifying the optimum reaction temperature. The successfully calcined powder was verified using X-ray diffraction spectroscopy (XRD) techniques. It was then ground and sieved through a 325-mesh (45 μm) screen before being pressed into rectangular bars. The synthesized conductive material was weighed out in 2-g portions and formed into bars measuring 6.5 mm × 32 mm × 2.5 mm using a steel mold through uniaxial pressing at 20 MPa. Subsequently, the compacted powder of the specimen bar was sintered at 1200 °C for 2 h before measuring the electrical conductivity using the 4-point DC method. Bulk density, porosity, structural image and thermal expansion coefficient were determined through the Archimedes water immersion technique, X-ray Tomographic Microscopy (XTM) by synchrotron, Scanning Electron Microscope (SEM) and dilatometer, respectively.

2.3. Analysis of characterizations and properties relevant to applications

The structural phases of automotive industrial waste, the transformed Fe_2O_3 waste powder and synthesized conductive materials were identified using X-ray diffraction (XRD, Bruker D2 PHASER) within an analytical 2-theta range of 10°–80°. A step time of 0.5 s per step and a step size of 0.02° per step were employed. Furthermore, quantitative analysis was conducted using software based on Topas analysis on a computer.

The elemental content was determined using an X-ray fluorescence spectrophotometer (XRF, PANalytical, Axios model) to confirm the elemental composition obtained from XRD analysis at room temperature under a vacuum system. All results will be used to determine the correct dosage of the mixture.

The most suitable reaction temperature and weight loss of the synthesized perovskite-type conductive material were determined using thermal analysis (STA, Mettler Toledo TGA/DSC1). An alumina crucible with alumina powder as a standard was employed. The analysis was conducted in the temperature range of 25–1200 °C with a heating rate of 10 °C/min under normal atmosphere and an airflow rate of 20 ml/min.

Initial electrical conductivity measurements were performed using a 4-point probe system (Ossila) on the sample surface, with a needle distance of 1.270 mm. A maximum voltage of 10 V and the target current of 1000 microamps were applied and repeatedly measured 25 times at room temperature. Afterwards, the electrical conductivity of the sintered rectangular bar sample was measured from 50 °C to 800 °C using the four-probe DC method. This method involves applying a DC current (I) between the outer two probes and measuring the resulting voltage drop across the inner two probes. All data was collected and measured in an air atmosphere at a heating rate of 3 °C/min.

The thermal expansion coefficient (TEC) was measured using Netzsch 402 dilatometer. The temperature measurement was carried out from 30 to 1000 °C under an ambient atmosphere with a heating rate of 5 °C/min.

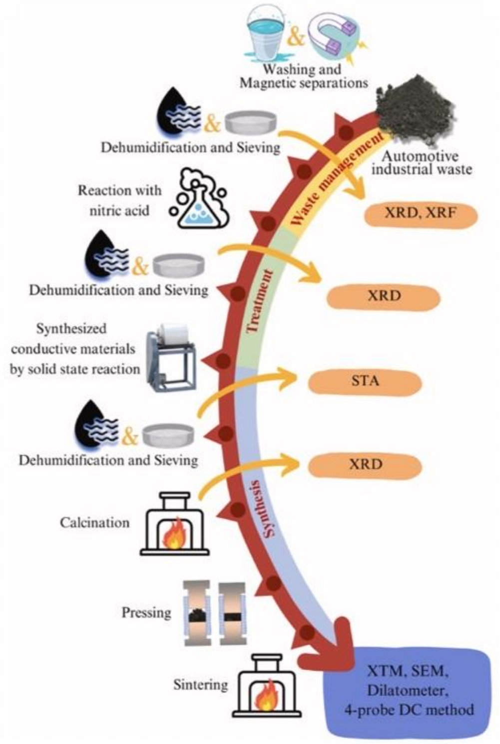

Fig. 1. The synthesis process of $LaNi_{1-x}Fe_xO_{3\pm\delta}$ perovskite-type conductive materials from automotive industrial waste.

The samples were compressed and sintered at 1200 °C. Subsequently, their microstructure was examined using FE-SEM MIRA3 (TESCAN) at beamline 6 at Synchrotron Light Research Institute (SLRI), Thailand with an electron beam energy level of 30 kV. This analysis was carried out in the secondary electron detector mode with magnifications of 5 kx, 30 kx and 100 kx. The particle size of the conductive materials was measured using the Martin's diameter method in ImageJ software [19].

SR-XTM was carried out at beamline 1.2W at Synchrotron Light Research Institute (SLRI), Thailand. For tomography data collection, the samples were stabilized with the paraffin wax within the sample holder and mounted on the rotary stage. The synchrotron light source operated at 1.2 GeV and 150 mA to minimize artifacts. Polychromatic X-rays were attenuated using a 200 μm thick aluminum foil with a mean energy of about 11.5 keV. A lens-coupled microscope and a scientific CMOS camera (2560x2160 pixels, 16 bit) were used, providing an optical performance with a pixel size of 1.44 μm. In a typical tomography scan, X-ray projections were collected for a 180° rotation with angular increments of 0.1°. Data pre-processing, background normalization and CT reconstruction were performed using Octopus Reconstruction software. The resulting tomograms were visualized in 3D volumes using Drishti software. The experimental procedures are shown in Fig. 1.

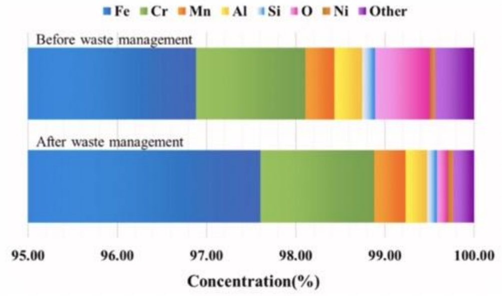

Fig. 2. XRF results of automotive industrial waste before and after waste management processes.

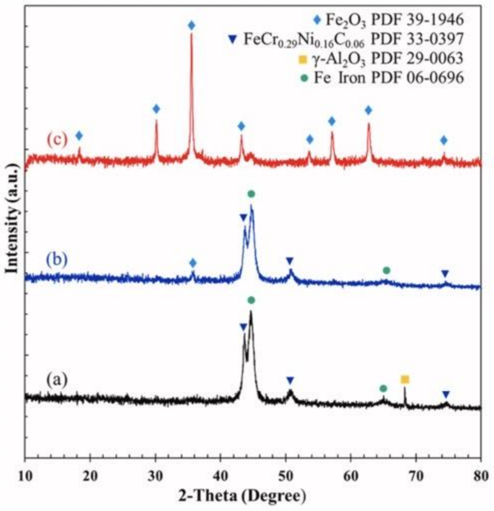

Fig. 3. XRD pattern of Fe-chemical compositions (3a) Before waste management (3b) After waste management and (3c) Waste treatment after reaction with nitric acid.

3. Results and discussion

3.1. The result of Fe-waste preparation and transformation to Fe_2O_3 by HNO_3 acid etching method

The XRF elemental analysis results of the Fe-waste before and after treatment are shown in Fig. 2. Prior to treatment, it was found that the automotive industrial waste had a high iron percentage of 96.88 %. Chromium (Cr), manganese (Mn), silicon (Si) and nickel (Ni)-fillers intended to improve some qualities of automobile parts were also found in quantities of 1.23 %, 0.33 %, 0.15 % and 0.06 %, respectively. Additionally, aluminum and oxygen were found, both of which are byproducts of the alumina complex (Al_2O_3), a mixture of ceramic abrasive powder. The iron concentration in automotive waste was found to be as high as 97.61 % after three passes of magnetic separation and washing in water, which is an increase of 0.73 % compared to before treatment. The leaching process was unable to remove the Cr, Mn, Si and Ni elements. It is evident that the quantities of these substances before and after leaching were similar. This may be attributed to the deliberate addition of these elements to steel to enhance its structure and improve its properties. As a result, it cannot be removed by water and cannot be separated by a magnet. However, the quantities of aluminum, oxygen and other contaminants significantly decreased as a result of washing with water and separating the magnetic powder through magnetic suction. This process effectively removes alumina abrasive powder and dust contaminants.

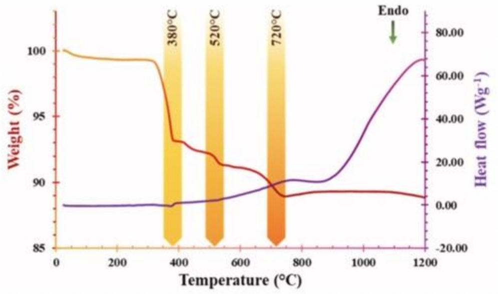

Fig. 4. The predictive reaction temperature of LaNi$_{1-x}$Fe$_x$O$_{3\pm\delta}$ synthesized substance.

The XRF analysis results are in alignment with and corroborated by the chemical composition analysis via XRD, as illustrated in Fig. 3. It was found that the Fe-waste before treatment (Fig. 3a) consisted of four main phases: Fe-Iron (JCPDS no. 06–0696) with peaks around 2θ values of approximately 45° and 65°, as well as 304-stainless steel austenite $FeCr_{0.29}Ni_{0.16}C_{0.06}$ phase (JCPDS No. 33–0397) was detected at 2θ values around 43°, 51° and 75°. These two phases are the main phases of Fe-rich waste by partially adding some elements to improve their properties. Furthermore, alumina abrasive powder (JCPDS No. 29–0063) was detected at 2θ of 68°, a finding consistent with XRF elemental analysis, which identified the presence of aluminum and oxygen. After water washing and magnetic separation (Fig. 3b), it was found that the alumina polishing powder detected at 2θ equal to 68 had disappeared. While treating or washing with water, iron can undergo oxidation due to the presence of oxygen in the water and air. Subsequently, the drying temperature of the waste powder triggers a chemical reaction, partially converting iron into iron oxide compounds. Therefore, the peak of iron oxide with JCPDS no. 39–1946 occurred at 2θ of 35°. However, the main phase of Fe-waste after treatment is still presented as Fe-iron with the same structure as Fe-waste before treatment.

The results of chemical composition analysis by XRD technique of Fe-waste treated with nitric acid (HNO_3) are shown in Fig. 3c. Only a single phase of the iron oxide compound with JCPDS no. 39–1946 was found in the XRD result pattern. This result is attributed to the complete chemical reaction between iron and nitric acid, resulting in the formation of a new phase of iron oxide, as predicted in Eq. (1) by following [2]:

$$2Fe_{(s)} + HNO_{3(l)} + 3H_2O_{(l)} \longrightarrow Fe_2O_{3(s)} + NH_{3(g)} + H_2O_{(g)} + H_2O_{2(g)} \quad (1)$$

The results of this chemical reaction can be achieved by heating it to approximately 100 °C. Besides transforming iron into iron oxide completely, this chemical reaction also produces useful by-products including Ammonia (NH_3), water (H_2O) and Hydrogen peroxide (H_2O_2). NH_3 is released during the reaction, which can be utilized for a wide range of applications as a fuel, working fluid, refrigerant, hydrogen carrier, fertilizer, feedstock, chemical, cleaning agent and many more [20]. Water itself is an important resource used for sustaining life. Hydrogen peroxide (H_2O_2) is also important in current research, often used for killing bacteria found in biological systems including being a foaming stimulant in cement, plaster, sound-absorbing materials, porous

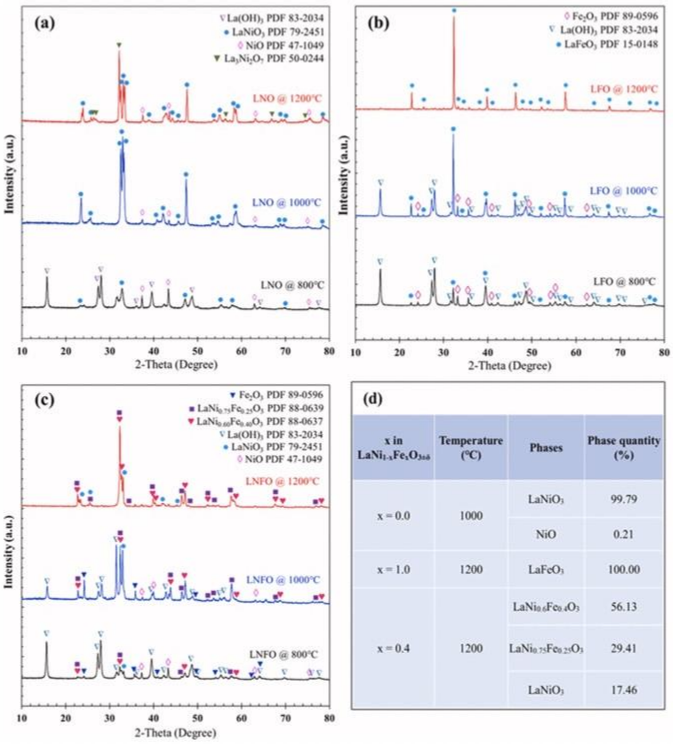

x in $LaNi_{1-x}Fe_xO_{3\pm\delta}$	Temperature (°C)	Phases	Phase quantity (%)
x = 0.0	1000	$LaNiO_3$	99.79
		NiO	0.21
x = 1.0	1200	$LaFeO_3$	100.00
x = 0.4	1200	$LaNi_{0.6}Fe_{0.4}O_3$	56.13
		$LaNi_{0.75}Fe_{0.25}O_3$	29.41
		$LaNiO_3$	17.46

Fig. 5. The structural phase of calcined powder at 800–1200 °C (5a) $LaNiO_{3\pm\delta}$, (5b) $LaFeO_{3\pm\delta}$, (5c) $LaNi_{0.6}Fe_{0.4}O_{3\pm\delta}$ and (5d) Phase quantity of $LaNi_{1\text{-}x}Fe_xO_{3\pm\delta}$ (with x = 0, 0.4 and 1).

materials and lightweight materials [21].

3.2. The result of analysis of characterizations and properties relevant to applications

3.2.1. Optimum temperature of synthesizing $LaNi_{1\text{-}x}Fe_xO_{3\pm\delta}$ compounds

The synthesized $LaNi_{1\text{-}x}Fe_xO_{3\pm\delta}$ conductive powder via solid-state reaction technique was analyzed by using STA (TGA-DTA techniques) as shown in Fig. 4. In the endothermic thermogravimetric analysis of the synthesized conductive powder, three distinct temperature points were observed and identified at around 380 °C, 520 °C and 720 °C. These temperatures correspond to stages of thermal degradation and collectively result in a total weight loss of 11 %. The observed reaction temperatures are linked to the strong endothermic reaction caused by the substantial physical water adsorption capacity of La_2O_3. This remarkable adsorption capability masks the exothermic reactions necessary for the formation of synthesized $LaNi_{1\text{-}x}Fe_xO_{3\pm\delta}$ conductive materials. Consequently, these exothermic reactions are not discernible in the STA graph. However, there are two primary temperature ranges associated with the endothermic reactions induced by La_2O_3. In the initial temperature range of 300–600 °C, the endothermic reactions involve the dehydration of $La(OH)_3$ into LaOOH (Lanthanum hydroxide-oxide), resulting in a cumulative weight loss of 8 %. These reactions occurred at temperatures of 380 °C and 520 °C, as defined in Eq. (2) [22,23].

$$La(OH)_{3(s)} \rightarrow LaO(OH)_{(s)} + H_2O_{(g)} \tag{2}$$

Eq. (3) [22,23] represents the complete endothermic reaction of LaOOH dehydration to La_2O_3 within a second temperature range of 600–800 °C. This reaction leads to a cumulative weight loss of 3 %.

$$2LaO(OH)_{(s)} \rightarrow La_2O_{3(s)} + H_2O_{(g)} \tag{3}$$

Although the final temperature investigated occurred at 720 °C and it is a dehydration reaction caused by the adsorption of La_2O_3 from traditional solid-state reaction synthesis process, the actual calcining will be studied in the temperature range of 800–1200 °C. Due to the large amount of chemicals utilized, the actual calcining process in a laboratory demands higher temperatures to complete the chemical reaction.

3.2.2. The structural characteristics of $LaNi_{1\text{-}x}Fe_xO_{3\pm\delta}$ calcined powder

Utilizing STA to analyze the reaction between the compounds $LaNi_{1\text{-}x}Fe_xO_{3\pm\delta}$, it was observed that the reaction terminated at approximately 800 °C, signifying the onset of the calcination process starting between 800 °C and 1200 °C. The powder was burned within the previously mentioned temperature range after the raw materials had been mixed according to the estimated proportions. Subsequently, the structural characteristics of the calcined powder were examined using XRD, and the results are presented in Fig. 5a-c.

Fig. 5a shows the XRD structural phase analysis of $LaNi_{1\text{-}x}Fe_xO_{3\pm\delta}$ (when x = 0). The results of calcination at 800 °C indicate that the precursors of NiO (JCPDS no. 47–1049) and $La(OH)_3$ (JCPDS no.

83–2034) are still present, indicating that the chemical reaction has not yet completed. However, NiO and $La(OH)_3$ starting materials are capable of undergoing partial chemical reactions after calcination at 800 °C, resulting in the formation of a new conductive phase substance. This can be observed through the detection of $LaNiO_{3\pm\delta}$ (JCPDS no. 79–2451) conductive phase. While calcining at temperatures ranging from 1000 to 1200 °C, the analysis results are the same. The $La(OH)_3$ precursor has completely disappeared due to the chemical reaction, resulting in the complete formation of the $LaNiO_{3\pm\delta}$ conductive phase. However, the NiO precursor is still present due to incomplete chemical reactions. Weighing is challenging and imprecise because the $La(OH)_3$ precursor quickly absorbs moisture, leading to an actual weight lower than the theoretically calculated value. As a result, there is an excess of NiO reactant left over from the reaction. According to the Topas Quantitative Phase Analysis using the Rietveld Refinement Method, the amount of the $LaNiO_{3\pm\delta}$ conductive phase (Rhombo.H.axes lattice with $a = b = 5.4573$, $c = 13.1462$ Å) and the NiO precursor (Cubic lattice with $a = b = c = 4.1771$ Å) remaining from the reaction was found to be 99.79 % and 0.21 %, respectively. It can be concluded that the electrically conductive compound $LaNiO_{3\pm\delta}$ is completely formed when calcined at a temperature of 1000 °C.

Fig. 5b displays the XRD phase analysis results of $LaNi_{1\text{-}x}Fe_xO_{3\pm\delta}$ (when $x = 1$). The results indicate that calcination at 800 °C still presents the Fe_2O_3 precursor peak (JCPDS no. 89–0596), derived from automotive industrial waste, and the peak of the $La(OH)_3$ precursor phase (JCPDS no. 83–2034). The presence of the $La(OH)_3$ precursor phase is attributed to the hygroscopic nature of La_2O_3 during the synthesis process [22]. Additionally, a new substance of $LaFeO_{3\pm\delta}$ phase (JCPDS no. 15–0148) was discovered, resulting from a chemical reaction involving all the precursors. At 1000 °C, peaks of Fe_2O_3 and $La(OH)_3$ precursors were still detected, indicating an incomplete chemical reaction. However, some interactions resulted in more pronounced $LaFeO_{3\pm\delta}$ peaks. After calcination at 1200 °C, the peaks of $La(OH)_3$ and Fe_2O_3 completely reacted to form single phases of 100 % $LaFeO_{3\pm\delta}$ with an orthorhombic lattice ($a = 5.556$ Å, $b = 5.565$ Å, $c = 7.862$ Å).

Fig. 5c shows the XRD phase analysis results of $LaNi_{1\text{-}x}Fe_xO_{3\pm\delta}$ with $x = 0.4$. The results indicated that at a calcination temperature of 800 °C, all precursor peaks of Fe_2O_3 (JCPDS No. 89–0596), NiO (JCPDS No. 47–1049) and the $La(OH)_3$ phase (JCPDS No. 83–2034) were detected in the XRD pattern, suggesting an incomplete chemical reaction. However, three new conductive phases of $LaNiO_{3\pm\delta}$ (JCPDS no. 79–2451), $LaNi_{0.6}Fe_{0.4}O_{3\pm\delta}$ (JCPDS no. 88-0.37) and $LaNi_{0.75}Fe_{0.25}O_{3\pm\delta}$ (JCPDS no. 88–0639) were detected and the quantity of each phase can be known by using TOPAS software as shown in Fig. 5d. All the above phases are products from the chemical reaction of precursors, but the calcination temperature of 800 °C is too low to allow for a chemical reaction to occur and result in a complete transformation into a new conductive phase. At a calcination temperature of 1000 °C, the same phase peaks were observed as those at 800 °C. A higher calcination temperature led to a reduction in precursor peaks and promoted further chemical reactions. Consequently, the peaks corresponding to the product substances of $LaNiO_{3\pm\delta}$, $LaNi_{0.6}Fe_{0.4}O_{3\pm\delta}$ and $LaNi_{0.75}Fe_{0.25}O_{3\pm\delta}$ were detected with greater clarity. At the calcined temperature of 1200 °C, the precursor peaks of $La(OH)_3$, NiO and Fe_2O_3 were fully transformed into conductive phases of $LaNiO_{3\pm\delta}$, $LaNi_{0.6}Fe_{0.4}O_{3\pm\delta}$ and $LaNi_{0.75}Fe_{0.25}O_{3\pm\delta}$. It was found that the reactants were able to react and change the structure to $LaNi_{0.6}Fe_{0.4}O_{3\pm\delta}$ with an Rhombo.H.axes lattice ($a = b = 5.5047$ Å, $c = 13.2642$ Å) in the highest amount of 53.13 %, which is the desired high-efficiency conductive phase. The temperature and synthesized conditions cannot produce a single phase of $LaNi_{0.6}Fe_{0.4}O_{3\pm\delta}$. Instead, both conductive phases of $LaNiO_{3\pm\delta}$ and $LaNi_{0.75}Fe_{0.25}O_{3\pm\delta}$ were found in amounts of 17.46 % and 29.41 %, respectively. However, there are guidelines for single-phase synthesis by lowering the calcination temperature below 1000 °C, but the calcination process can take up to 24 h to create a single phase. Because oxides containing Ni ions in $LaNi_{1\text{-}x}Fe_xO_{3\pm\delta}$ synthetic materials with x less than or equal to 0.4 have a lower valence than 3+, they are sensitive to temperatures higher than 1000 °C, easily causing a second phase [14,25].

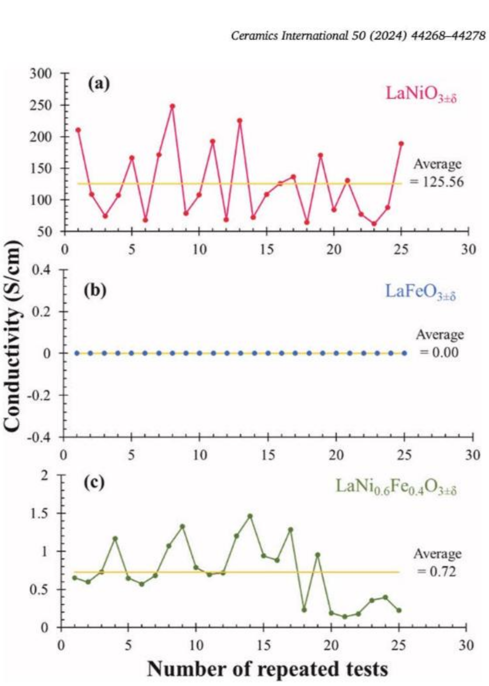

Fig. 6. Initial electrical conductivity of synthetic materials (6a) $LaNiO_{3\pm\delta}$ (6b) $LaFeO_{3\pm\delta}$ and (6c) $LaNi_{0.6}Fe_{0.4}O_{3\pm\delta}$ by using a surface 4-point probe at room temperature.

3.2.3. Electrical conductivity properties of $LaNi_{1\text{-}x}Fe_xO_{3\pm\delta}$ perovskite-type conductive materials

The initial electrical conductivity of $LaNi_{1\text{-}x}Fe_xO_{3\pm\delta}$ (with $x = 0$, 0.4 and 1) perovskite-type conducting specimens was measured using a surface 4-point probe at room temperature. The measurements were conducted with each sample tested 25 times under consistent recording conditions. Preliminary conductivity measurements were conducted with an oscilloscope at room temperature to eliminate variables not suitable for measurement with the 4-probe DC method. The 4-probe DC method has complicated preparation, requires time, and involves high temperature for testing. Moreover, materials with low electrical conductivity are not suitable for use as cathode materials in SOFCs. According to the testing results, $LaNiO_{3\pm\delta}$ and $LaNi_{0.6}Fe_{0.4}O_{3\pm\delta}$ exhibited electrical conductivity at room temperature, with average conductivities of approximately 125.6 S/cm (Fig. 6a) and 0.7235 S/cm (Fig. 6b), respectively. Both types of workpieces were then further measured for electrical conductivity using the 4-probe DC method, which extends the results to measure the electrical conductivity of specimens under simulated actual operating conditions and utilization.

However, the electrical conductivity of $LaFeO_{3\pm\delta}$ at room temperature is shown in Fig. 6b. Preliminary analysis results indicated that no electrical current was detected from the workpiece. Therefore, it may be concluded that these materials either lack electrical conductivity or exhibit very limited conductivity. Documents reporting the results consistently show that $LaFeO_{3\pm\delta}$ exhibit very low electrical conductivity, even at high temperatures [14,25]. As there are other better options available, it is not considered for further detailed using the 4-probe DC

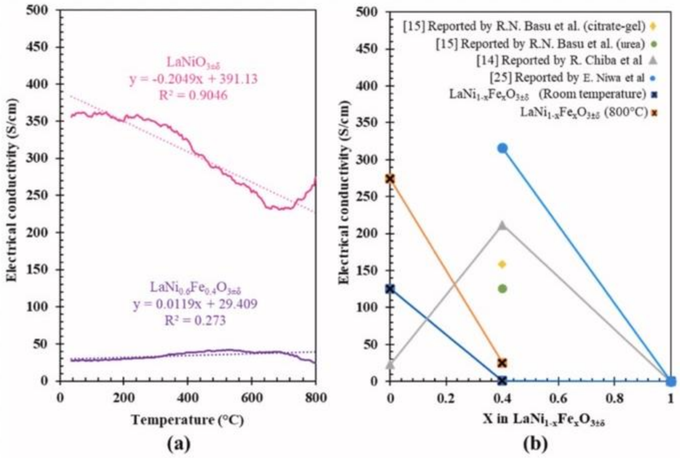

Fig. 7. Electrical conductivity of synthetic materials (7a) using 4-probe DC method at a temperature range of 50–800 °C of $LaNiO_{3\pm\delta}$ and $LaNi_{0.6}Fe_{0.4}O_{3\pm\delta}$. (7b) The electrical conductivity of $LaNi_{1\text{-}x}Fe_xO_{3\pm\delta}$ at room temperature and 800 °C compared the electrical conductivity reported.

method. The electrical conductivity behavior of perovskite materials depends on the outermost electrons, which affects the strength of the adsorption of oxygen and transition metal ions [26]. According to the research of L. Zeng et al. [27], $LaNi_{1\text{-}x}Fe_xO_{3\pm\delta}$ exhibits a rhombohedral structure when Fe^{3+} ions replace some of the Ni^{3+} ions, causing structural distortion and creating oxygen vacancies. This effect is particularly pronounced when $0 \leq x \leq 0.4$, due to the smaller atomic size of Fe^{3+} compared to Ni^{3+}. As a result, there is an increase in the partial reduction of Fe^{3+} to Fe^{2+}, which influences the oxygen absorption capacity and significantly enhances electrical conductivity [28,29]. And it has the highest electrical conductivity when 40 % Fe is doped into the position of Ni. However, if more than 40 % is doped in $LaNi_{1\text{-}x}Fe_xO_{3\pm\delta}$, the structure will change to Orthorhombic. When comparing the Fe^{2+}/Fe^{3+} ratio, it was observed that $LaNi_{1\text{-}x}Fe_xO_{3\pm\delta}$ with 1 mol of Fe substitution exhibited a ratio indicating that Fe^{2+} was only partially present, suggesting partial doping with Fe. This resulted in a reduced ability to absorb oxygen. Therefore, $LaNi_{1\text{-}x}Fe_xO_{3\pm\delta}$ at x = 1 has such low electrical conductivity that it cannot be measured by the 4-probe method at room temperature [27].

Although $LaFeO_{3\pm\delta}$ synthetic materials lack conductive properties and are not commonly used as an electrode, they are highly efficient when used as a sensor for detecting gases of NO_2, CO, acetylene and ethylene [24,30]. However, it is evident that previous research has not utilized waste materials for synthesizing $LaFeO_{3\pm\delta}$ and applying it in sensor applications. Therefore, this research shows promise, and further testing is necessary to confirm the sensors performance.

Fig. 7a shows the electrical conductivity of synthetic conductive materials using the 4-probe DC method. $LaNiO_{3\pm\delta}$ conductivity was measured in great detail using the 4-probe DC technique between 50 and 800 °C, revealing metallic conductivity behavior. The highest conductivity recorded for $LaNiO_{3\pm\delta}$ is 362 S/cm at 150 °C as depicted in Fig. 7a. This observation indicates that conductivity decreases as temperature increases, a phenomenon explained by Crystal Field Theory [31]. $LaNiO_{3\pm\delta}$ consists of a low-spin configuration of Ni^{3+} (with a double degenerate level of 1 and a triply degenerate level of 6), which is consistent with its metallic conductive behavior. In contrast, $LaFeO_{3\pm\delta}$ exhibits a high-spin configuration for Fe^{3+}, characterized as a charge-transfer insulator with localized electron configuration (double degenerate level of 2 and triply degenerate level of 3). Consequently, the $LaNi_{1\text{-}x}Fe_xO_{3\pm\delta}$ system shows a composition-controlled metal–insulator transition at x = 0.3, likely due to the enhanced disorder effect caused by replacing Ni with Fe in the system. Due to its mixed conductivity behavior, the electrical conductivity of $LaNi_{0.6}Fe_{0.4}O_{3\pm\delta}$ may be relatively constant [32]. When Ni is replaced by Fe with x = 0.4, as illustrated in Fig. 7b, the conduction behavior of $LaNi_{0.6}Fe_{0.4}O_{3\pm\delta}$ specimen changes from metallic to semiconductive characteristics.

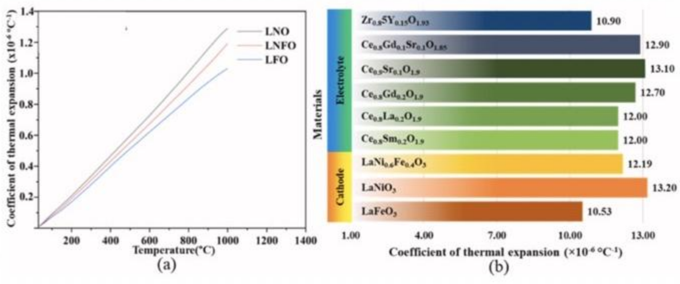

Fig. 8. The coefficient of thermal expansion of (8a) $LaNi_{1\text{-}x}Fe_xO_{3\pm\delta}$ (with x = 0, 0.4 and 1) synthesized compounds and (8b) the currently SOFC electrolyte materials.

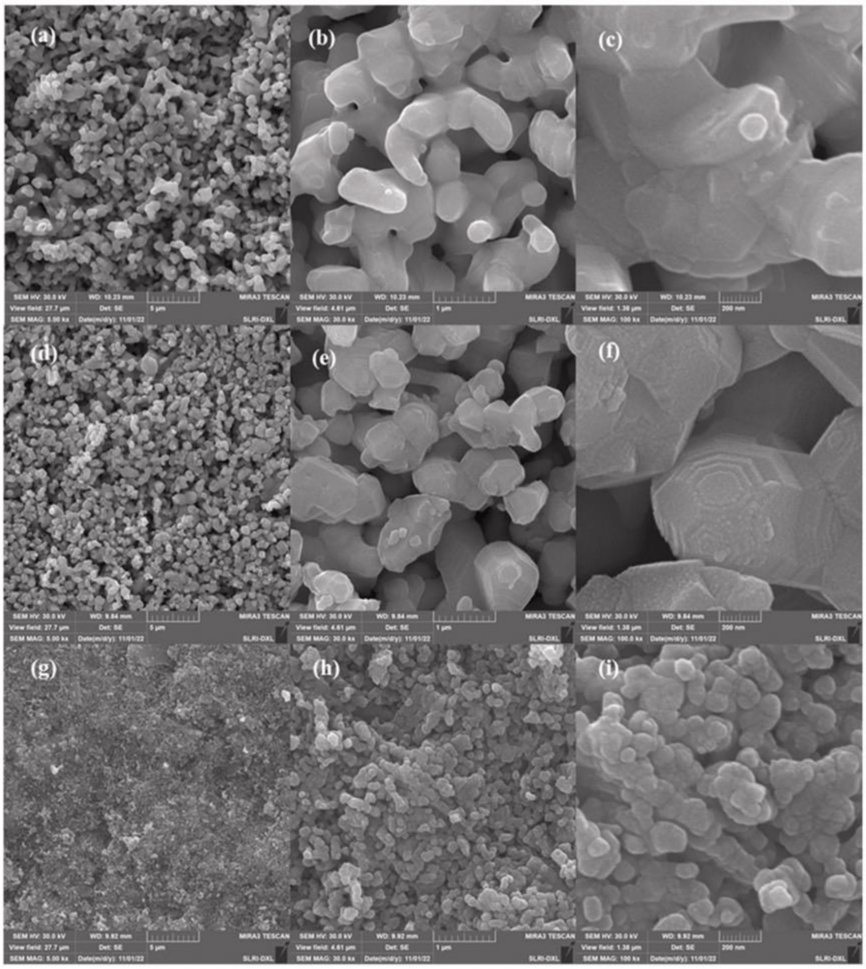

Fig. 9. SEM images of $LaNi_{1-X}Fe_XO_{3\pm\delta}$ perovskite-type conducting materials (9a) $LaNiO_{3\pm\delta}$ 5kx, (9b) $LaNiO_{3\pm\delta}$ 30kx, (9c) $LaNiO_{3\pm\delta}$ 100kx, (9d) $LaFeO_{3\pm\delta}$ 5kx, (9e) $LaFeO_{3\pm\delta}$ 30kx, (9f) $LaFeO_{3\pm\delta}$ 100kx, (9g) $LaNi_{0.6}Fe_{0.4}O_{3\pm\delta}$ 5kx, (9h) $LaNi_{0.6}Fe_{0.4}O_{3\pm\delta}$ 30kx and (9i) $LaNi_{0.6}Fe_{0.4}O_{3\pm\delta}$ 100kx.

Semiconductive conducting behavior occurs in the low-temperature range, from room temperature up to 800 °C. It is observed that as the temperature increases, electrical conductivity gradually rises. The $LaNi_{0.6}Fe_{0.4}O_{3\pm\delta}$ synthesized material exhibits a maximum electrical conductivity of 42 S/cm. Although the $LaNi_{0.6}Fe_{0.4}O_{3\pm\delta}$ synthetic materials do not exhibit highly conductive behavior in this research, they are suitable for use as cathode materials in IT-SOFC. Fig. 7b shows the electrical conductivity at room temperature and 800 °C, obtained from waste from the automotive parts industry as a precursor. Compared with previously reported results at 800 °C, $LaNi_{0.6}Fe_{0.4}O_{3\pm\delta}$ has a significantly lower electrical conductivity than other reported materials. This is the result of not being able to synthesize them into a single phase. However, the synthesized $LaNi_{0.6}Fe_{0.4}O_{3\pm\delta}$ conductive specimen cannot be produced as a single phase under inappropriate synthesis conditions. The resultant material exhibits poorer electrical conductivity compared to the cathode materials currently utilized in IT-SOFCs. Therefore, if the experiment is carried out and the conditions are suitable for the synthesis of $LaNi_{0.6}Fe_{0.4}O_{3\pm\delta}$ material with a 100 % single phase, the electrical conductivity will increase to approximately around 300 S/cm at an operating temperature 800 °C [25].

3.2.4. The coefficient of thermal expansion results of $LaNi_{1-x}Fe_xO_{3\pm\delta}$ conductive perovskite-type materials

The thermal expansion coefficient (TEC) of $LaNi_{1-x}Fe_xO_{3\pm\delta}$ (with $x = 0$, 0.4 and 1) synthesized samples as measured using a dilatometer is shown in Fig. 8. The establishment of test conditions is based on references related to IT-SOFC applications, which operate within a temperature range from room temperature up to 1000 °C. From the experiment, it was found that the thermal expansion coefficients of $LaNiO_{3\pm\delta}$, $LaNi_{0.6}Fe_{0.4}O_{3\pm\delta}$ and $LaFeO_{3\pm\delta}$ were 13.02×10^{-6}, 12.19×10^{-6} and

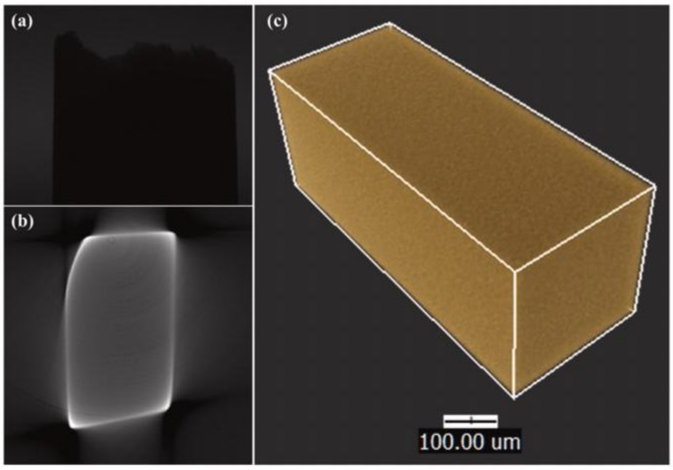

Fig. 10. The porosity analysis of $LaNi_{0.6}Fe_{0.4}O_{3\pm\delta}$ using synchrotron radiation XTM technique (10a) Projection image from micro-CT of XTM (10b) Reconstructed image from Octopus reconstruction program (10c) 3D image from Drishti program (inside - cross section).

10.53×10^{-6} °C^{-1}, respectively. The substitution of Fe in the Ni-position as in the experiment from Fig. 8a, resulted in a decreasing value in the thermal expansion coefficient of the $LaNi_{0.6}Fe_{0.4}O_{3\pm\delta}$ perovskite electrically conductive material. Additionally, when Ni is completely replaced with Fe at 100 %, the thermal expansion coefficient value decreases and is lower than that of other workpieces. Therefore, it can be concluded that iron processed from automobile manufacturing waste is arranged into a unique structure with qualities that help reduce the thermal expansion coefficient of the $LaNi_{1-x}Fe_xO_{3\pm\delta}$ conductive perovskite structure. Additionally, as demonstrated in Fig. 8b [33,34], the substitution by Fe-waste results in a thermal expansion coefficient that is comparable to the electrolyte materials currently employed in IT-SOFCs such as Yttria-stabilized zirconia (YSZ) and CeO_2 (with other dopants of La, Sm Gd and Sr). The materials will be strong, long-lasting, and stable to the environment inside the cell since they have similar coefficients of thermal expansion after the cell has been assembled. Low thermal expansion coefficients do not compromise cell performance at IT-SOFC operating temperatures, contributing to a longer service life.

3.2.5. Microstructure and porosity analysis of conductive perovskite-type materials by synchrotron light source

The results of a cross-sectional microstructure study using the FE-SEM technique $LaNi_{1-x}Fe_xO_{3\pm\delta}$ (with x = 0, 0.4 and 1) sintered at 1200 °C are presented in Fig. 9. The microstructure study findings indicate that $LaNi_{1-x}Fe_xO_{3\pm\delta}$ material exhibits a consistent, porous microstructure composed of grains with uniform size distribution and a pellet-like shape. The FE-SEM images clearly show that the $LaNiO_{3\pm\delta}$ and $LaFeO_{3\pm\delta}$ materials have larger grain sizes. The image J analysis technique also supports and indicates that $LaNiO_{3\pm\delta}$ and $LaFeO_{3\pm\delta}$ materials have average grain sizes of approximately 0.62 μm and 0.57 μm, respectively. However, after adding Fe dopant to $LaNiO_{3\pm\delta}$, the grain size of $LaNi_{0.6}Fe_{0.4}O_{3\pm\delta}$ is significantly smaller than that of other synthesized compositions with an average grain size of 0.13 μm. The introduction of Fe dopant into $LaNiO_{3\pm\delta}$ reduces the average particle size, which decreases with increasing Fe content due to lattice distortion caused by the addition of Fe ions. This lattice distortion can lead to reduced nucleation and grain growth rates in Fe-doped $LaNiO_{3\pm\delta}$. The reduction in average crystallized size suggests an improvement in crystallinity [35,36]. Consequently, the grain and particle sizes are smaller. This not only increases the contact surface area [25,36,37], but also affects pore size. Smaller particle sizes lead to a more closely connected and arranged structure, resulting in smaller pores [37,38]. This is consistent with the research of A. Z. Mahmoud et al. which showed that doping Fe into ZnO resulted in smaller particle sizes, resulting in a smaller pore size, higher surface area and higher percentage of porosity [15,30]. Porous properties are desirable in the cathode material for IT-SOFC (Intermediate Temperature Solid Oxide Fuel Cell) applications. In addition to electrical conductivity, the cathode material needs to be porous to facilitate the easy flow of fuel and oxygen gases into the IT-SOFC unit cell, promoting efficient chemical reactions and enhancing fuel cell efficiency and electricity generation. This is in accordance with the findings from the synchrotron light source analysis, as demonstrated in Fig. 10.

The micro-CT images of SR-XTM of $LaNi_{0.6}Fe_{0.4}O_{3\pm\delta}$ sample obtained from a synchrotron light source are displayed in Fig. 10(a–c). The solid black contrast in Fig. 10a denotes a high sample density, which can be attributed to the orientation of small particles. As a result, low X-ray transmittance leads to ring artifacts in reconstructed images using the Octopus reconstruction program, as shown in Fig. 10b. When irradiated, light scattering occurs due to the metallic composition of the synthesized sample. The XTM technique's resolution restrictions, restrict analysis of porosity smaller than 0.72 μm, preventing determination of the sample's overall porosity. This relationship between particle size and porosity is confirmed by the arrangement of small particles, resulting in the formation of small pores. This is evident in the distribution of tiny bright spots scattered throughout the workpiece, as depicted in Fig. 10c with a 3D image from the Drishti program (inside cross-section).

4. Conclusions

Iron powder waste (Fe) from the automotive parts industry was treated to reduce contamination before being used as a starting material in this process. Upon exposure to air, the iron powder can oxidize, forming oxide compounds. Therefore, it was synthesized by reacting with HNO_3 acid, resulting in Fe_2O_3. The next step was to study whether this Fe_2O_3 is effective enough to be used as a precursor for the synthesis of advanced materials. In this research, Fe_2O_3 derived from automotive parts industry waste was used as a precursor for synthesizing perovskite structural materials. $LaNi_{1-x}Fe_xO_{3\pm\delta}$ (with x = 0, 0.4 and 1) was investigated for use as a cathode in SOFCs, which are high-energy cells that are not toxic to the environment. This study includes the analysis of physical properties analysis and testing of key material properties. The chemical composition, microstructure, thermal expansion coefficient and electrical conductivity suggest that waste from the automotive parts industry can be used, exhibiting properties similar to those reported in previous research. This approach not only mitigates environmental pollution from waste but also enhances its value. The compounds synthesized from automotive industrial waste may find application as IT-SOFC cathode materials or serve other purposes. For instance, the $LaFeO_{3\pm\delta}$ compound can be employed as a gas sensing material, necessitating further investigation into its additional properties.

Funding

This research was financially supported by the Suranaree University of Technology Research and Development Fund.

Availability of data and materials

The datasets generated during and/or analyzed during the current study are available from the corresponding author on reasonable request.

Ethical approval

Not applicable.

Consent to participate

Not applicable.

Consent to publish

The participant has consented to the submission of the case report to the journal.

CRediT authorship contribution statement

Siriwan Chokkha: Methodology, Data curation, Conceptualization. **Aphisit Tonsanthia:** Methodology. **Natthawat Chuprasoet:** Methodology. **Kraiwut Rukkachat:** Methodology.

Declaration of competing interest

The authors declare no competing interests.

Acknowledgements

This research was financially supported by the Suranaree University of Technology Research and Development Fund (Thailand). We express gratitude to Suranaree University of Technology (SUT) for facilitating a portion of the research. Additionally, we extend our thanks to the Synchrotron Light Research Institute (SLRI), particularly Dr. Pattanaphong Janphuang for FE-SEM analysis at beamline 6, and Dr. Phakkhananan Pakawanit for SR-XTM conducted at beamline 1.2W.

References

[1] Thailand Automotive Institute, Thailand automotive Institute annual report. https://www.thaiauto.or.th/2020/about-us/Accomplishment.asp, 2021. (Accessed 17 October 2022), 2021.

[2] C.H. Natthawat, S. Thanasak, B. Rattana, C.H. Siriwan, The transformation of automotive industrial waste to useful iron compounds, Suranaree J. Sci. Technol. 29 (1) (2021) 010097, 1-6, https://ird.sut.ac.th/journal/sjst/#/los/manuscript/25211.

[3] J. Khanam, MdR. Hasan, B. Biswas, ShA. Jahan, N. Sharmin, S. Ahmed, ShMd Al-Reza, Development of ceramic grade red iron oxide pigment from waste iron source, Heliyon 9 (2023) e12854, https://doi.org/10.1016/j.heliyon.2023.e12854.

[4] A. Biswasd, A.K. Patraa, S. Sarkara, D. Dasb, D. Chattopadhyay, S. De, Synthesis of highly magnetic iron oxide nanomaterials from waste iron by one-step approach, Colloids Surf., A 589 (2020) 1244, https://doi.org/10.1016/j.colsurfa.2020.124420.

[5] K. Lee, S. Hajra, M. Sahu, H.J. Kim, Colossal dielectric response, multiferroic properties, and gas sensing characteristics of the rare earth orthoferrite $LaFeO_3$ ceramics, J. Alloys Compd. 882 (2021) 160634, https://doi.org/10.1016/j.jallcom.2021.160634.

[6] M. Sorescu, T. Xu, A. Hannan, Initial stage growth mechanism of $LaFeO_3$ perovskite through magnetomechanical ball-milling of Lanthanum and iron oxides, Am. J. Mater. Sci. 1 (1) (2011) 57–66. http://article.sapub.org/pdf/10.5923.j.materials.20110101.09.pdf.

[7] J. Peng, J. Huang, X.L. Wu, Y.W. Xu, H. Chen, X. Li, Solid oxide fuel cell (SOFC) performance evaluation, fault diagnosis and health control: a review, J. Power Sources 505 (2021) 230058, https://doi.org/10.1016/j.jpowsour.2021.230058.

[8] V. Sinha, S. Mondal, Recent development on performance modelling and fault diagnosis of fuel cell systems, Int. J. Dynam. Control (2017), https://doi.org/10.1007/s40435-017-0328-4.

[9] S. Hussain, L. Yangping, Review of solid oxide fuel cell materials: cathode, anode, and electrolyte, Energy Transitions (2020), https://doi.org/10.1007/s41825-020-00029-8.

[10] S. Dwivedi, Solid oxide fuel cell: materials for anode, cathode and electrolyte, Int. J. Hydrogen Energy (2019), https://doi.org/10.1016/j.ijhydene.2019.11.234.

[11] A.J.A. Aziza, N.A. Baharuddina, M.R. Somalua, A. Muchtara, Review of composite cathodes for intermediate-temperature solid oxide fuel cell applications, Ceram. Int. (2020), https://doi.org/10.1016/j.ceramint.2020.06.176.

[12] A.A. Yaremchenko, B.I. Arias-Serrano, K. Zakharchuk, J.R. Frade, Perovskite-like $LaNiO_{3-\delta}$ as oxygen electrode material for solid oxide electrolysis cells, ECS Trans. 91 (1) (2019) 2399–2408, https://doi.org/10.1149/09101.2399ecst.

[13] F. Lu, M. Yang, Y. Shi, C. Wu, X. Jia, H. He, J. Su, M. Chao, B. Cai, Application of a negative thermal expansion oxide in SOFC cathode, Ceram. Int. 47 (2021) 1095–1100, https://doi.org/10.1016/j.ceramint.2020.08.225.

[14] R. Chiba, F. Yoshimura, Y. Sakurai, An investigation of $LaNi_{1-x}Fe_xO$ as a cathode material for solid oxide fuel cells, Solid State Ionics 124 (1999) 281–288, https://doi.org/10.1016/S0167-2738(99)00222-2.

[15] R.N. Basu, F. Tietz, E. Wessel, H.P. Buchkremer, D. Stover, Microstructure and electrical conductivity of $LaNi_{0.6}Fe_{0.4}O_3$ prepared by combustion synthesis routes, Mater. Res. Bull. 39 (2004) 1335–1345, https://doi.org/10.1016/j.materresbull.2004.03.015.

[16] K. Vidal, A. Morán-Ruiz, A. Larrañaga, J.M. Porras-Vázquez, P.R. Slater, M. I. Arriortu, Characterization of $LaNi_{0.6}Fe_{0.4}O_3$ perovskite synthesized by glycine-nitrate combustion method, Solid State Ionics 269 (2015) 24–29, https://doi.org/10.1016/j.ssi.2014.11.002.

[17] J. Richter, P. Holtappels, Th Graule, T. Nakamura, Ludwig J. Gauckler, Materials design for perovskite SOFC cathodes, Monatsh. Chem. 140 (2009) 985–999, https://doi.org/10.1007/s00706-009-0153-3.

[18] S.U. Rehman, R.H. Song, T.H. Lim, J.E. Hong, S.B. Lee, Parametric study on electrodeposition of a nanofibrous $LaCoO_3$ SOFC cathode, Ceram. Int. (2020), https://doi.org/10.1016/j.ceramint.2020.10.141.

[19] D. Wang, L.S. Fan, Particle Characterization and Behavior Relevant to Fluidized Bed Combustion and Gasification Systems, Woodhead Publishing Limited, 2013, https://doi.org/10.1533/9780857098801.1.42.

[20] D. Erdemir, I. Dincer, A perspective on the use of ammonia as a clean fuel: challenges and solutions, Int. J. Energy Res. (2020) 1–8, https://doi.org/10.1002/er.6232.

[21] B.J. Juven, M.D. Pierson, Antibacterial effects of hydrogen peroxide and methods for its detection and quantitation, J. Food Protect. 59 (11) (1996) 1233–1241, https://doi.org/10.4315/0362-028X-59.11.1233.

[22] P. Fleming, R.A. Farrell, J.D. Holmes, M.A. Morris, The rapid formation of $La(OH)_3$ from La_2O_3 powders on exposure to water vapor, J. Am. Ceram. Soc. 93 (4) (2010) 1187–1194, https://doi.org/10.1111/j.1551-2916.2009.03564.x.

[23] M. Sorescu, T. Xu, J.D. Burnett, J.A. Aitken, Initial stage growth mechanism of $LaFeO_3$ perovskite through magneto mechanical ball-milling of Lanthanum and iron oxides, J. Mater. Sci. 46 (2011) 6709–6717, https://doi.org/10.1007/s10853-011-5625-2.

[24] N. Sharma, H.S. Kushwaha, S.K. Sharma, K. Sachdev, Fabrication of $LaFeO_3$ and rGO-$LaFeO_3$ microspheres-based gas sensors for detection of NO_2 and CO, RSC Adv. 10 (2020) 1297–1308. https://pubs.rsc.org/en/content/articlepdf/2020/ra/c9ra09460a.

[25] N. Eiki, U. Chie, M. Erina, O. Takeshi, H. Takuya, Conductivity and sintering property of $LaNi_{1-x}Fe_xO_3$ ceramics prepared by Pechini method, Solid State Ionics 201 (2011) 87–93, https://doi.org/10.1016/j.ssi.2011.08.004.

[26] M.A. Peña, J.L.G. Fierro, Chemical structures and performance of perovskite oxides, Chem. Rev. 101 (2017) 1981, https://doi.org/10.1021/cr980129f, 2001.

[27] L. Zeng, T. Peng, H. Sun, J. Yang, Y. Li, Y. Qin, Fe-doped $LaNi_{1-x}Fe_xO_3$ perovskite oxides for enhanced visible-light-driven photocatalytic activity, J. Solid State Chem. 297 (2021) 122033, https://doi.org/10.1016/j.jssc.2021.122033.

[28] Zh Yong, J Bin, Y Mengjiao, L Peiwen, L Wei, Zh Xuejun, Formaldehyde-sensing properties of $LaFeO_3$ particles synthesized by citrate sol–gel method, J. Sol. Gel Sci. Technol 79 (2016) 167–175. https://link.springer.com/article/10.1007/s10971-016-4025-0.

[29] N. Eiki, U. Chie, M. Junichiro, H. Takuya, Oxygen nonstoichiometry and electrical conductivity of $LaNi_{0.6}Fe_{0.4}O_{3-\delta}$ at high temperatures under various oxygen partial pressures, Solid State Ionics 274 (2015) 119–122, https://doi.org/10.1016/j.ssi.2015.02.022.

[30] A.A. Alharbia, A. Sackmanna, U. Weimara, N. Bârsan, A highly selective sensor to acetylene and ethylene based on $LaFeO_3$, Sensor. Actuator. B Chem. 303 (2020) 127, https://doi.org/10.1016/j.snb.2019.127204.

[31] M.A. Komorynsky, Companion, Crystal Field Splitting Diagrams, J. Chem. Educ. 41 (5) (1964) 257. https://doi.org/10.1021/ed041p257.

[32] A. Yoshinobu, H. Naoyuki, K. Masaki, H. Ken, U. Tetsuya, Experimental validation of high electrical conductivity in Ni-rich $LaNi_{1-x}Fe_xO_3$ solid solutions ($x \leq 0.4$) in high-temperature oxidizing atmospheres, Mater. Adv. (2021), https://doi.org/10.1039/D0MA00983K.

[33] S. Sameshima, M. Kawaminami, Y. Hirata, Thermal expansion of rare-earth-doped ceria ceramics, J. Ceram. Soc. Jpn. 110 (7) (2002) 597–600, https://doi.org/10.2109/jcersj.110.597.

[34] F. Tietz, Thermal expansion of SOFC materials, Ionics 5 (1999) 129–139, https://doi.org/10.1007/BF02375916.

[35] A.Z. Mahmoud, E.M.M. Ibrahim, L. Galal, E.R. Shaaban, Influence of Fe substitution on structural morphological and magnetic properties of $Zn_{1-x}Fe_xO$ thin films to various applications, Sohag J. Sci. 8 (1) (2023) 91–98, https://doi.org/10.21608/sjsci.2022.153658.1017.

[36] C. Torres-Sanchez, J. McLaughlin, R. Bonallo, Effect of Pore Size, Morphology and Orientation on the Bulk Stiffness of a Porous Ti35Nb4Sn Alloy, JMEPEG, 2018, https://doi.org/10.1007/s11665-018-3380-0.

[37] Y Luo, X Wang, Q Qian, Q Chen, Studies on B sites in Fe-doped $LaNiO_3$ perovskite for SCR of NO_x with H_2, Int. J. Hydrogen Energy 39 (2014) 15836–15843. https://doi.org/10.1016/j.ijhydene.2014.07.135.

[38] D. Gou, X. An, R. Yang, Characterization of the evolution of pore structure with particle breakage during compaction, Miner. Eng. (2022), https://doi.org/10.1016/j.mineng.2022.107751.